TÜBİTAK

Turkish Journal of Earth Sciences

http://journals.tubitak.gov.tr/earth/

Research Article

Turkish J Earth Sci
(2015) 24: 72-98
© TÜBİTAK
doi:10.3906/yer-1407-5

Provenance, diagenesis, tectonic setting, and geochemistry of Hawkesbury Sandstone (Middle Triassic), southern Sydney Basin, Australia

Samir Mahmoud ZAID[1]*, Fahad AL GAHTANI[2]

[1]Department of Geology, Faculty of Sciences, Zagazig University, Zagazig, Egypt
[2]Ministry of Petroleum and Mineral Resources, Riyadh, Saudi Arabia

Received: 07.07.2014 • **Accepted:** 23.10.2014 • **Published Online:** 02.01.2015 • **Printed:** 30.01.2015

Abstract: The Hawkesbury Sandstone is an important groundwater reservoir in the southern part of the Sydney Basin, Australia. However, its diagenesis and provenance and its impact in reservoir quality are virtually unknown. The present study aims to reconstruct the parent rock assemblages of the Hawkesbury Sandstone, their tectonic provenance, and the physiographic conditions under which these sediments were deposited. Samples from the EAW 18a and EDEN 115 field representing the Middle Triassic Hawkesbury Sandstone were studied using a combination of petrographic, mineralogical, and geochemical techniques. The Hawkesbury Sandstone is yellowish brown in color, siliceous, and partly calcareous; it originated as sands were deposited in fluvial channels. Texturally, Hawkesbury Sandstone is medium- to coarse-grained, mature, and moderately well sorted. Scarcity of feldspars indicates that the rock is extensively recycled from a distant source. Hawkesbury Sandstone has an average framework composition of $Q_{92.07}F_{0.31}R_{7.62}$, and 95.9% of the quartz grains are monocrystalline. The Hawkesbury Sandstone is mostly quartz arenites with subordinate sublithic arenites, and bulk-rock geochemistry supports the petrographic results. Petrographic and geochemical data of the sandstones indicate that they were derived from craton interior to quartzose recycled sedimentary rocks and deposited in a passive continental margin of a syn-rift basin. The cratonic Lachlan Orogen is the main source of Hawkesbury Sandstone. The chemical index of alteration, plagioclase index of alteration, and chemical index of weathering values (3.41–87.03) of the Hawkesbury Sandstone indicate low-moderate to high weathering, either of the original source or during transport before deposition, and may reflect low-relief and humid climatic conditions in the source area. Diagenetic features include compaction: kaolinite, silica, mixed-layer clays, siderite, illite, and ankerite cementation with minor iron-oxide, dolomite, chlorite, and calcite cements. Silica dissolution, grain replacement, and carbonate dissolution greatly enhance the petrophysical properties of many sandstone samples.

Key words: Provenance, Hawkesbury Sandstone, Sydney Basin, Australia

1. Introduction

The Middle Triassic Hawkesbury Sandstone is an important groundwater reservoir in the Illawarra district of New South Wales, Australia, including the EAW 18a and EDEN 115 field (Rust and Jones, 1987; Miall and Jones, 2003; Figure 1). The Middle Triassic Hawkesbury Sandstone served as one of the primary sources of groundwater, while the Middle Triassic shale (Mittagong Formation) represents the excellent capping rocks for these reservoirs. Almost 15% of the groundwater is produced from the Hawkesbury Sandstone (Rust and Jones, 1987). In the southern Sydney Basin, the Middle Triassic Hawkesbury Sandstone has a wide geographic distribution, either exposed or subsurface.

Provenance studies of clastic sedimentary rocks often aim to reveal the composition and geological evolution of the sediment source areas and to constrain the tectonic setting of the depositional basin. Previous works have revealed that the chemical composition of clastic sediments is a function of a complex interplay of several variables, including the source rock composition, the extent of weathering, transportation, and diagenesis (Taylor and McLennan, 1985; Bhatia and Crook, 1986). However, the tectonic setting of the sedimentary basin may play a predominant role over other factors, because different tectonic settings can provide different kinds of source materials with variable chemical signatures (Bhatia, 1983; Pettijohn et al., 1987; Chamley, 1990; Armstrong-Altrin and Verma, 2005). For instance, the sediments in the passive continental margin tend to have more stable features (rich in Si, low in Mg and Fe, etc.), whereas the sediments in the back arc basin are always rich in mafic rather than felsic signatures (Bhatia and Crook, 1986). Many attempts have been made to refine provenance

* Correspondence: samir_zaid75@yahoo.com

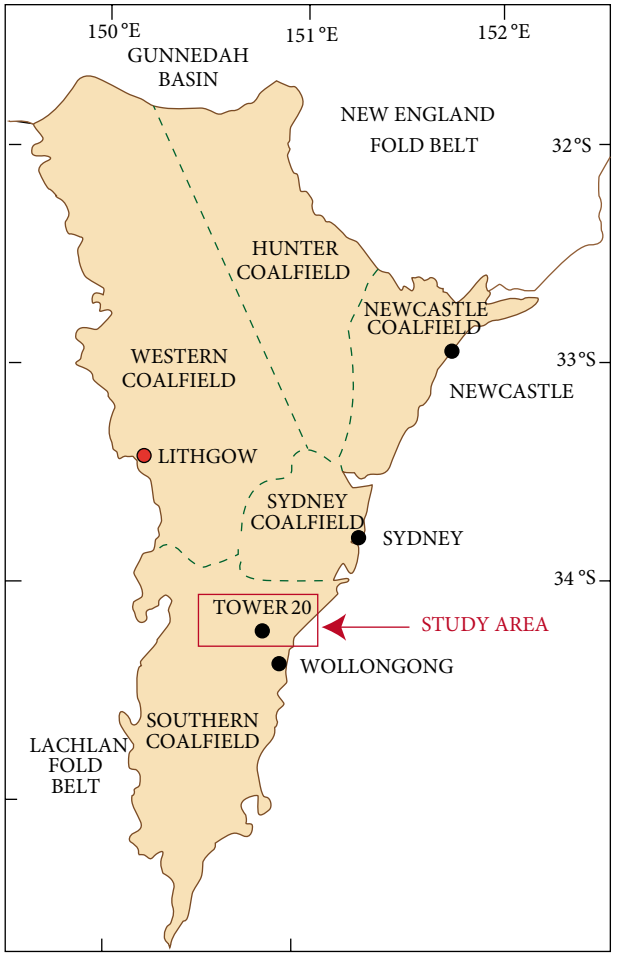

Figure 1. Location of the Sydney Basin and the coalfields within it (from Grevenitz et al., 2003).

models using the framework composition (Suttner et al., 1981; Dickinson et al., 1983; Weltje et al., 1998) and geochemical features (Bhatia, 1983; Roser and Korsch, 1986, 1988; Suttner and Dutta, 1986; Kroonenberg, 1994; Armstrong-Altrin et al., 2004, 2012, 2013).

Significant contributions have been made by several studies in relation to the regional geology, sedimentology, and tectonic evolution of the Hawkesbury Sandstone (e.g., Conolly, 1969; Standard, 1969; Conolly and Ferm, 1971; Conaghan and Jones, 1975; Ashley and Duncan, 1977; Conaghan, 1980; Herbert, 1980; Jones and Rust, 1983; Rust and Jones, 1987; Miall and Jones, 2003; Gentz, 2006; Johnson, 2006). However, no studies of the geochemistry and tectonic setting have been made.

The present work was conducted on the outcrop and 2 wells (EAW 18a and EDEN 115), aiming to reconstruct the parent rock assemblages of the Hawkesbury Sandstone, their tectonic provenance, and the physiographic conditions under which these sediments were deposited, using an integrated provenance approach involving modal analysis and bulk-rock geochemistry data from the outcrop and the 2 wells (EAW 18a and EDEN 115; Tables 1 and 2).

2. Geologic setting

The stratigraphic column of the southern coalfield includes the rock units from the Upper Permian to the Middle Triassic normally encountered in the Sydney Basin (Figure 2). The Hawkesbury Sandstone conformably overlies the Newport Formation of the Narrabeen Group and conformably underlies the Mittagong Formation of the Wianamatta Group (Herbert, 1980). The average thickness of the Hawkesbury Sandstone is around 230 m (Rust and Jones, 1987).

Unidirectional paleoflow in the sandstone, its freshwater biota, and abundant mudrock intraclasts indicate fluvial deposition. Sheet morphology, low paleocurrent variance, abundant erosion surfaces, and the paucity of in situ mudrocks point to a braided fluvial system. Three facies assemblages have been recognized: stratified sandstone, massive sandstone, and a minor mudrock assemblage (Rust and Jones, 1987; Miall and Jones, 2003). Massive sandstone is widespread in the Hawkesbury Sandstone, occurring in structureless to faintly parallel-stratified sandstone beds (Rust and Jones, 1987; Miall and Jones, 2003). Massive sandstone beds, horizontally stratified and ripple-cross-laminated, are included in the stratified sandstone assemblage. Massive sandstone has a thickness of 0.5 m in sheet-like units. Cross-stratal sets occur in both trough and planar forms (Rust and Jones, 1987). Mudrock facies are minor in the Hawkesbury Sandstone. Standard (1969) showed that the thickness of units of the mudrock assemblage reaches up to 12 m. Conolly (1969) and Conolly and Ferm (1971) suggested that the Hawkesbury Sandstone was deposited in a marine barrier to tidal delta system. Ashley and Duncan (1977) proposed that the Hawkesbury Sandstone was deposited in an aeolian environment. Conaghan and Jones (1975), Conaghan (1980), Rust and Jones (1987), and Miall and Jones (2003) indicated that the deposition of the Hawkesbury Sandstone was by a large braided river, similar to the modern Brahmaputra River.

The Sydney Basin forms the southernmost part of the Bowen–Gunnedah–Sydney Basin system (Figure 1), an asymmetric retroarc foreland basin overlying the junction of the Lachlan–Tasman and New England Fold Belts (Veevers et al., 1994). Formation of the Bowen–Gunnedah–Sydney Basin system began in the Early Permian with rifting of the eroded Lachlan Fold Belt and Tamworth Block of the New England Fold Belt together with subsidence related to the cooling of the magmatic arc. This led to the encroachment of marine waters into the basin and the deposition of a series of alternating shallow

Table 1. Textural data of the Hawkesbury Sandstone.

	Sample no.	Avg. grain size	Grain roundness	Grain sorting	Grain contact
Hawkesbury Sandstone	S6	F-M	SR	M-Ws	C > P
	S7	F-M	SA-SR	Ws	P > L
	S8	F	SR	Ws	P > L
	S9	F-M	SA-SR	M-Ws	C > P
	S10	C	R	M-Ws	C > P
	S11	M-C	SA-SR	Ws	F > P
	S12	VC	SR	Ms	P > L
	EAW1	F	SA-SR	P-Ms	F > P
	EAW2	C	SR-R	VWs	C > P
	EAW3	F-M	R	Ms	C > P
	EAW4	C	SR	Ws	C > P
	EAW5	F-M	SR	Ws	F > P
	EAW7	C	SR-R	M-Ws	C > P
	EAW8	C	SR-R	P-Ms	C > P
	EAW9	F	SR	M-Ws	C > P
	EAW10	M-C	SR	M-Ws	C > P
	EDEN1	C	SR-R	P-Ms	F > P
	EDEN2	M-C	SR-R	P-Ms	P > L
	EDEN3	C	R	Ms	F > P
	EDEN4	F	SR	Ms	C > P
	EDEN5	F	SR-R	M-Ws	C > P
	EDEN6	C	SR	Ws	C > P
	EDEN7	C	R	VPs	C > P
	EDEN8	C	SR-R	Ms	P > L
	EDEN9	C	SR	M-Ws	P > L
	EDEN10	F-M	SR-R	P-Ms	C > P
	EDEN11	C	R	Ps	P > L
	EDEN12	C	SA	P-Ms	P > L
	EDEN13	C	R	Ws	F > P
	EDEN14	C	SA	Ms	P > L
	EDEN15	C	SR-R	Ms	P > L
	EDEN16	C	SR-R	M-Ws	C > P

F = Fine-grained; F-M = fine to medium; M-C = medium to coarse; C = coarse-grained; VC = very coarse-grained; SA = subangular; SA-SR = subangular to subrounded; SR-R = subrounded to rounded; R = rounded; VPs = very poorly sorted; P-Ms = poorly to moderately sorted; Ms = moderately sorted; M-Ws = moderately to well sorted; Ws = well sorted; F > P= float > point contact; P > L= point > long contact; C > P = concave–convex > point contact.

marine and alluvial sequences, the latter including coal measures (Dehghani, 1994; Veevers et al., 1994; Bamberry et al., 1995; Veevers, 2006). During the Middle to Late Permian, the sequences gradually became dominated by fluvial and coal deposits; major regression in the Late Permian due to uplift of the New England Orogen resulted in the formation of a foreland basin and the development of swampy deltaic conditions that ultimately produced the extensive coal deposits of the Illawarra Coal Measures (Dehghani, 1994; Retallack, 1999; White and Saunders, 2005). The influx of material from the New England Fold Belt in the form of lacustrine, fluvial, and floodplain deposits of the overlying Narrabeen Group resulted in the cessation of coal deposition in the Early Triassic (Naughton and Terada, 1954; Dehghani, 1994; Saunders et al., 2005). Subsequent uplift and erosion exposed these rocks in highlands, generally westerly of the present coastline, to provide sources for the simple succession of Early (Narrabeen Group) and Middle (Hawkesbury Sandstone and Wianamatta Group) Triassic distinctive sedimentary layers deposited in the depression. Tilting of the region during this deposition changed source areas of the sediments, the Narrabeen Group being derived from the north and the overlying Hawkesbury Sandstone from southerly sources (Saunders et al., 2005).

3. Samples and methodology

The petrography of the Hawkesbury Sandstone was based on 32 samples. These samples were selected from the outcrop and from 2 wells (EAW 18a and EDEN 115). Thin sections prepared from 32 blue epoxy-impregnated samples were examined under a polarizing microscope. The amounts of detrital and diagenetic components, and pore types as well as the textural modal grain size and sorting parameters, were determined by counting 400 points in each of the 32 thin sections. The point counts were done using both Gazzi–Dickinson (Gazzi, 1966; Dickinson, 1970) and standard methods to minimize the dependence of rock composition on grain size (Ingersoll et al., 1984). Framework parameters (Ingersoll and Suczek, 1979) and detrital modes of the studied sandstone samples are given in Table 2.

The morphology and textural relationships among minerals were examined in 8 gold-coated samples with a scanning electron microscope (SEM) equipped with an energy-dispersive spectrometer (EDS), using an accelerating voltage of 10 kV. X-ray diffraction (XRD) analyses were performed for studied samples using a Philips (PW3710) diffractometer (Cu Kα radiation, 35 kV, 28.5 mA) to determine the percentage of each mineral in fine-grained samples and clay minerals in the sandstone samples (oriented samples of <2-μm clay fractions).

All studied samples were analyzed for major-element geochemistry. The major oxides were determined in

Table 2. Point-counted data and the derived QFL indices of the Hawkesbury Sandstone.

	S no.	Detrital mineralogy										Authigenic mineralogy											QFL%			QmFLt%				
												Carbonate cement				Authigenic clays													Po	Matrix
		Qm	Qp	KF	PF	Lp	Lv	Ls	Nop	I.O	Mu	Qz th	Sid	Cal	Ank	Dol	Ill	Ka	Chl	Mix	Qt	F	L	Qm	F	Lt		
Hawkesbury Sandstone	S6	59.5	2	0	0	0.3	0	7.6	0.3	0.7	0	6.4	0	0	0	0	3.2	5.2	0.3	14.5	88.62	0.00	11.38	85.73	0.00	14.27	18.1	5.1
	S7	67.9	2.1	0.2	0	0.3	0	2.8	0.4	0.5	0	6.1	0	0.2	0.2	0	1.7	6	1.7	9.9	95.50	0.27	4.23	92.63	0.27	7.09	11.5	20
	S8	65.7	1	0	0	0.2	0	7	0.6	1.3	0	3.3	0.1	0	0	0	0	8.5	1.3	11	90.26	0.00	9.74	88.90	0.00	11.10	8.6	12.2
	S9	53.3	1.8	0	0	0.3	0	17.3	0.4	0.5	0	5.8	0	0	0	0	4.5	8.9	2.1	5.1	75.79	0.00	24.21	73.31	0.00	26.69	11.2	9.4
	S10	64.1	2.4	0.5	0.1	0.2	0	0.7	0.3	0.5	0	7	0	0	0	0	4.5	13.4	0	6.3	97.79	0.88	1.32	94.26	0.88	4.85	19.3	4.9
	S11	64.7	2.2	0.2	0	0	0	14.3	0.7	0.8	0	6.9	0.1	0	0.1	0	2.9	5.1	0	2	82.19	0.25	17.57	79.48	0.25	20.27	1.6	8.4
	S12	69.7	2.6	0.3	0	0.1	0	6.4	0.8	1.1	0	7.3	0	0	0	0	2.1	7.5	0	2.1	91.40	0.38	8.22	88.12	0.38	11.50	6.4	5.3
	EAW1	49.7	2	0	0	0.1	0	13.2	0.8	0.8	0	5.2	1.5	0	13.2	5.4	1.3	3.6	0.7	2.5	79.54	0.00	20.46	76.46	0.00	23.54	0	8.1
	EAW2	75.1	3.1	0	0	0.2	0	2.9	0.2	0.2	0	8.2	1.1	0	0	0	0.1	5.7	0	3.2	96.19	0.00	3.81	92.37	0.00	7.63	3.9	5.1
	EAW3	47.6	3.3	0	0	0.2	0	15	0.1	0.4	0.4	4.9	9.4	0	0	0	0.2	14.4	0	4.1	77.00	0.00	23.00	72.01	0.00	27.99	0	18.7
	EAW4	56.3	2.7	0.3	0	0.4	0	2.6	0.2	0.5	0	6.1	1.1	0	0	0	0	25.1	0	4.7	94.70	0.48	4.82	90.37	0.48	9.15	16.8	13
	EAW5	58.5	2.4	0	0	0.3	0	2.6	0.1	0.1	0	6	2.4	0	0	0.4	0	22	0	5.2	95.45	0.00	4.55	91.69	0.00	8.31	13	14.2
	EAW7	65.8	3.2	0.4	0.1	0	0	6.1	0.1	0.3	0	7.2	0.9	0	0	0	0.2	13	0	2.7	91.27	0.66	8.07	87.04	0.66	12.30	11.7	4.2
	EAW8	41.8	2.2	0.5	0.1	0.3	0	1.5	0.1	0.2	3	3.7	6.3	0.6	0	0.6	2	24.3	0	12.8	94.83	1.29	3.88	90.09	1.29	8.62	0	39.1
	EAW9	56.8	2.3	0.5	0.1	0.2	0	1.7	0.1	0.1	1.8	3.9	3.3	0	0	0	0.7	19.8	0	8.7	95.94	0.97	3.08	92.21	0.97	6.82	0	29.2
	EAW10	61.7	2.5	0	0	0.1	0	2.1	0.1	0.1	0.2	6.1	2.7	0	0	0.1	1.3	19.4	0	3.6	96.69	0.00	3.31	92.92	0.00	7.08	3.2	21.1
	EDEN1	66.7	2.5	0	0	0	0	8.1	0.1	0.1	0	6.9	1.9	0	0	0	1.2	10	0	2.5	89.52	0.00	10.48	86.29	0.00	13.71	0.2	13.5
	EDEN2	71.7	3.4	0.4	0	0	0	1.9	0.1	0.3	0.2	7.2	0	0	0	0	1.3	10.4	0	3.1	97.03	0.52	2.45	92.64	0.52	6.85	14.2	0.6
	EDEN3	80	3.3	0	0	0	0	1	0.1	0.1	0	8	0	0	0	0	0.2	6.5	0	0.8	98.81	0.00	1.19	94.90	0.00	5.10	0	7.5
	EDEN4	57.1	2.7	0	0	0.2	0	4.3	0.2	0.5	0	6.2	0.2	0	0	0	0	23.9	0	4.7	93.00	0.00	7.00	88.80	0.00	11.20	19.1	9.5
	EDEN5	61.5	2.8	0	0	0	0	4.8	0.1	0.2	0	6.7	0	0	0	0	0	18.7	0	5.2	93.05	0.00	6.95	89.00	0.00	11.00	7.7	16.2
	EDEN6	62.1	3.1	0	0	0	0	14.5	0.1	0.1	0	6.9	0	0	0	0	2.6	7.4	0	3.2	81.81	0.00	18.19	77.92	0.00	22.08	0	13.2
	EDEN7	68.2	2.4	0	0	0	0	2.4	0.1	0.2	0	7.6	0.6	0	2.2	0	2.1	10	0	4.2	96.71	0.00	3.29	93.42	0.00	6.58	13.5	2.8
	EDEN8	24.4	2.7	0.5	0.1	0	0	0	0.1	0.3	2.4	1.2	15.3	0.6	0.9	0.6	2.6	31.1	0	17.2	97.83	2.17	0.00	88.09	2.17	9.75	0	50.9
	EDEN9	63.7	3.4	0.5	0.1	0.2	0	3.5	0.2	0.4	0	7	1.5	0	0.2	0	1.3	13.8	0	4.2	93.98	0.84	5.18	89.22	0.84	9.94	16.5	2.8
	EDEN10	74.8	2.9	0	0	0	0	2.4	0.1	0.2	0	8.3	1.2	0	0	0	0.6	9.3	0	0.2	97.00	0.00	3.00	93.38	0.00	6.62	3	7.1
	EDEN11	67	2.6	0	0	0.2	0	1.3	0.1	0.2	0	7.4	6.4	0	0	0	0.7	10.4	0	3.7	97.89	0.00	2.11	94.23	0.00	5.77	14.3	0.5
	EDEN12	29.1	2.7	0.3	0	0	0	6.7	0.2	0.4	1.7	0.5	15.7	0.8	0.8	1.6	0	31.8	0	7.7	81.96	0.77	17.27	75.00	0.77	24.23	0	39.5
	EDEN13	64.2	3.1	0.2	0	0	0	0.7	0.4	0.6	0	7.1	4.7	0	0	0.3	0	14.8	0	3.9	98.68	0.29	1.03	94.13	0.29	5.57	13.8	4.9
	EDEN14	70.2	3.1	0	0	0.1	0	3	0.1	0.1	0	7.6	12	0	0	0.5	0.4	2.7	0	0.2	95.94	0.00	4.06	91.88	0.00	8.12	2.5	0.8
	EDEN15	61.7	2.7	0	0	0.3	0	2.5	0.2	0.2	0	6.7	3	0	0	0	0.6	18	0	4.1	95.83	0.00	4.17	91.82	0.00	8.18	15.5	7.2
	EDEN16	75.5	2.4	0	0	0.1	0	4	0.6	1.9	0.2	8.5	3.5	0	0	0	0.3	2.5	0	0.5	95.00	0.00	5.00	92.07	0.00	7.93	3.3	0
Min.		24.4	1	0	0	0	0	0	0.1	0.1	0	0.5	0	0	0	0	0	2.5	0	0.2	75.7909	0	0	72.01	0	4.853	0	0
Max.		80	3.4	0.5	0.1	0.4	0	17.3	0.8	1.9	3	8.5	15.7	0.8	13.2	5.4	4.5	31.8	2.1	17.2	98.8138	2.166	24.21	94.9	2.17	27.99	19.3	50.9
Average		61.13	2.61	0.15	0.02	0.13	0.00	5.15	0.25	0.43	0.31	6.18	2.97	0.07	0.55	0.30	1.21	13.23	0.19	5.12	92.10	0.31	7.59	88.14	0.31	11.56	7.78	12.34

Qm = Monocrystalline quartz; Qp = polycrystalline quartz; KF = K-feldspar; PF = plagioclase-feldspar; Lp = plutonic lithic fragment; Lv = volcanic lithic fragment; Ls = sedimentary lithic fragment; M = mica; Nop = nonopaque; I.O = iron oxides; Mu = muscovite; Qz th = quartz overgrowth; Sid = siderite; Cal = calcite; Ank = ankerite; Dol = dolomite; Ill = illite; Ka = kaolinite; Chl = chlorite; Mix = mixed-layer clay; Po = point-counted porosity. Qt = Total quartz; F = feldspar; Lt = total lithic fragment; Qt = Qm + Qp; F = Pl + KF; L = Lp+ Lv + Ls; Lt = L + Qp.

Age			Group	Subgroup	Formation	Member
Triassic	Early and Middle		Wianamatta Group	Liverpool Subgroup	Ashfield Shale	
					Mittagong Formation	
					Hawkesbury Sandstone	
			Narrabeen Group	Gosford Subgroup	Newport Formation	
					Garie Formation	
				Clifton Subgroup	Bald Hill Claystone	
					Bulgo Sandstone	
					Stanwell Park Claystone	
					Scarborough Sandstone	
					WombarraClaystone	Otford Sandstone Member
					Coal Cliff Sandstone	
Permian	Late	Tetarian	Illawarra Coal Measures	Sydney Subgroup	Bulli Coal	
					Loddon Sandstone	
					Eckersley Formation	Balgownie Coal Member
						Lawrence Sandstone Member
						BurragorangClaystone
						Cape Horn Coal Member
						Hargrave Coal Member
						Woronora Coal Member
						Novice Sandstone Member
					Wongawilli Coal	
					Kembla Sandstone	
					Allans Creek Formation	American Creek Coal Member
					Darkes Forest Sandstone	
					Bargo Claystone	Austinmer Sandstone Member
					Tongarra Coal	
					Wilton Formation	Woonona Coal Member
				Cumberland Subgroup	Erins Vale Formation	Kulnura Marine Tongue
					Pheasant Nest Formation	Figtree Coal Member
						Unanderra Coal Member
						Tappitallee Mountain Tuff Member
						Berkeley Latite Member
						MinnamurraLatite Member
			Shoalhaven		Broughton Formation	
					Berry Formation	
					Nowra Sandstone	

Figure 2. Stratigraphy of Southern Coalfield (after Bamberry, 1992).

32 bulk samples using the X-ray fluorescence (XRF) spectrometry technique on fused beads (Rollinson, 1993). The correlation coefficient was obtained for the chemical data using the method of Davis (1986). XRF, XRD, and SEM-EDS analyses were performed at the laboratory of the National Research Center of Egypt. Analytical precision was better than 5% for the major oxides. Loss of ignition (LOI) was estimated by firing dried samples at 1000 °C for 2 h. Total iron was expressed as Fe_2O_3. Major-element data were recalculated to an anhydrous (LOI-free) basis and adjusted to 100% before using them in various diagrams.

4. Results

4.1. Sandstone petrofacies and texture

The Middle Triassic Hawkesbury Sandstone is composed of sandstones and less common siltstone and shale. The analyzed sandstone samples of the Hawkesbury Sandstone Formation are medium- to coarse-grained, subangular to subrounded, and moderately to poorly sorted (Table 1). All types of major grain contact, including float, point, long, and concave –convex, are present. However, an abundance of point contact was noted. Sandstone classification was made using the Dott–McBride scheme (Figure 3). The Hawkesbury sandstones are mostly quartz arenites with subordinate sublithic arenites and have an average framework composition of $Q_{92.07}F_{0.31}R_{7.62.}$ The framework grains are mainly quartz (69.54% of the rock volume) and less frequently of feldspar, rock fragments, and heavy minerals (avg. 6.15%). Framework constituents account for 86% of the rock, and the matrix and cement constitute about 14%. The matrix partly consists of clay minerals and detrital constituents. The observed types of cement include silica, siderite, calcite, ankerite, and dolomite (Table 2; Figure 4). Average existing pore space constitutes 7.84% of the rock (Table 2).

Quartz is the most abundant framework grain in the sandstones, constituting an average 92.07% of rock volume. The quartz grains are commonly subangular to subrounded in shape (Figure 4a). Most of the quartz grains show multiple deformation fractures (Figures 4b and 4c). Among quartz grains, Qm (95.9 vol.%) is dominant over Qp. Most of the Qm grains have undulatory extinction. Some of quartz grains contain inclusions of rutile, zircon, and tourmaline (Figure 4d). Long, point, and concavo-convex contacts are common (Figure 4b) and are caused by pressure solution and compaction. Some quartz grains display syntaxial overgrowths (Figure 4e), and some others are corroded at their margins (Figures 4c and 4f). Heavy minerals, mica flakes (Figure 4d), and clay minerals (kaolinite, illite, mixed clay, and chlorite) also exist (Figures 4e–4g). Mica and heavy minerals (rutile, zircon, and tourmaline) appear in accessory quantities (<1.0%; Table 2).

Feldspars (avg.: 0.31%) are mostly absent in many thin sections (Table 2). They are subangular and clear of inclusions. Orthoclase, microcline, and perthite are the most common varieties. K-feldspar (K) (avg. 0.15%) dominates over plagioclase (avg. 0.02%) and is mostly orthoclase and microperthite, with fewer microcline grains. Most feldspar grains are altered, which implies a high degree of chemical weathering. Plagioclase is rare and occurs as altered grains.

Rock fragment include chert, carbonate (shell), and metamorphic (Qp) fragments (Figures 4b and 4h). Volcanic (Lv) and plutonic (Lp) fragments are completely absent in Hawkesbury sandstones. Generally, the fragments are subrounded; however, a few rounded clasts are observed. The absence of feldspars in most samples indicates that the rock is extensively recycled and derived from old sedimentary rocks.

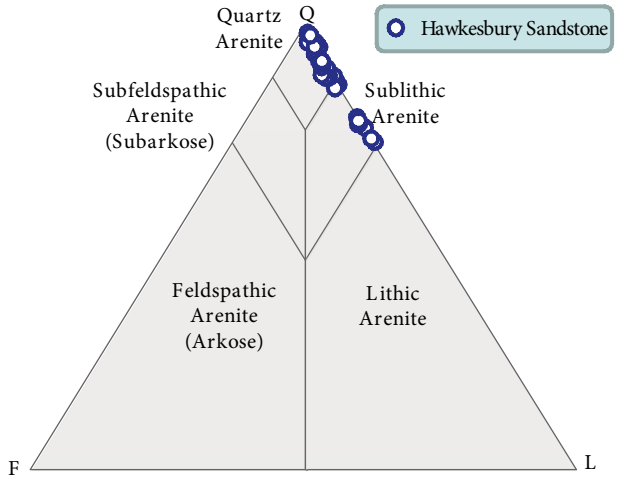

Figure 3. QFL triangular diagram shows the classification of the Hawkesbury sandstones, modified from Dott (1964) and McBride (1963).

Lithic fragments are recorded in the majority of samples (Figures 4d, 4h, and 4i). They range from 0.0% to 17.7% with an average of 5.28%. They include chert, siltstone, claystone, granitic fragments, and metamorphic fragments in decreasing order of abundance. Volcanic fragments (Lv) are completely absent in these sandstones. Compositionally, the most abundant types of lithic fragments are chert fragments (Figures 4d and 4h), hematitic claystone, and hematitic siltstone (Figures 4c and 4i). Generally, the fragments are subrounded; however, a few rounded clasts are observed. Lithic plutonic (Lp) fragments are rare. They include clasts of quartz and feldspar and are granitic in origin.

Muscovite is a minor accessory grain type within the samples. It ranges from 0.0% to 3.0% with an average of 0.31%. Grains are fine-medium to coarse-grained and replaced by siderite cement in some samples (Figure 4d). The regionally metamorphosed rocks and granite are the main source of mica.

Heavy minerals form a minor constituent (less than 0.7%) of the sandstones and include rounded to well-rounded grains of zircon, rutile, tourmaline, and opaque minerals (Table 2). The dominant accessory heavy minerals are composed mainly of opaque minerals (ilmenite, magnetite, and hematite). Grains of heavy minerals are very fine and show moderate abrasion. The assemblage is suggestive of a mixed sedimentary (reworked), igneous, and metamorphic source. Cementing materials occurring

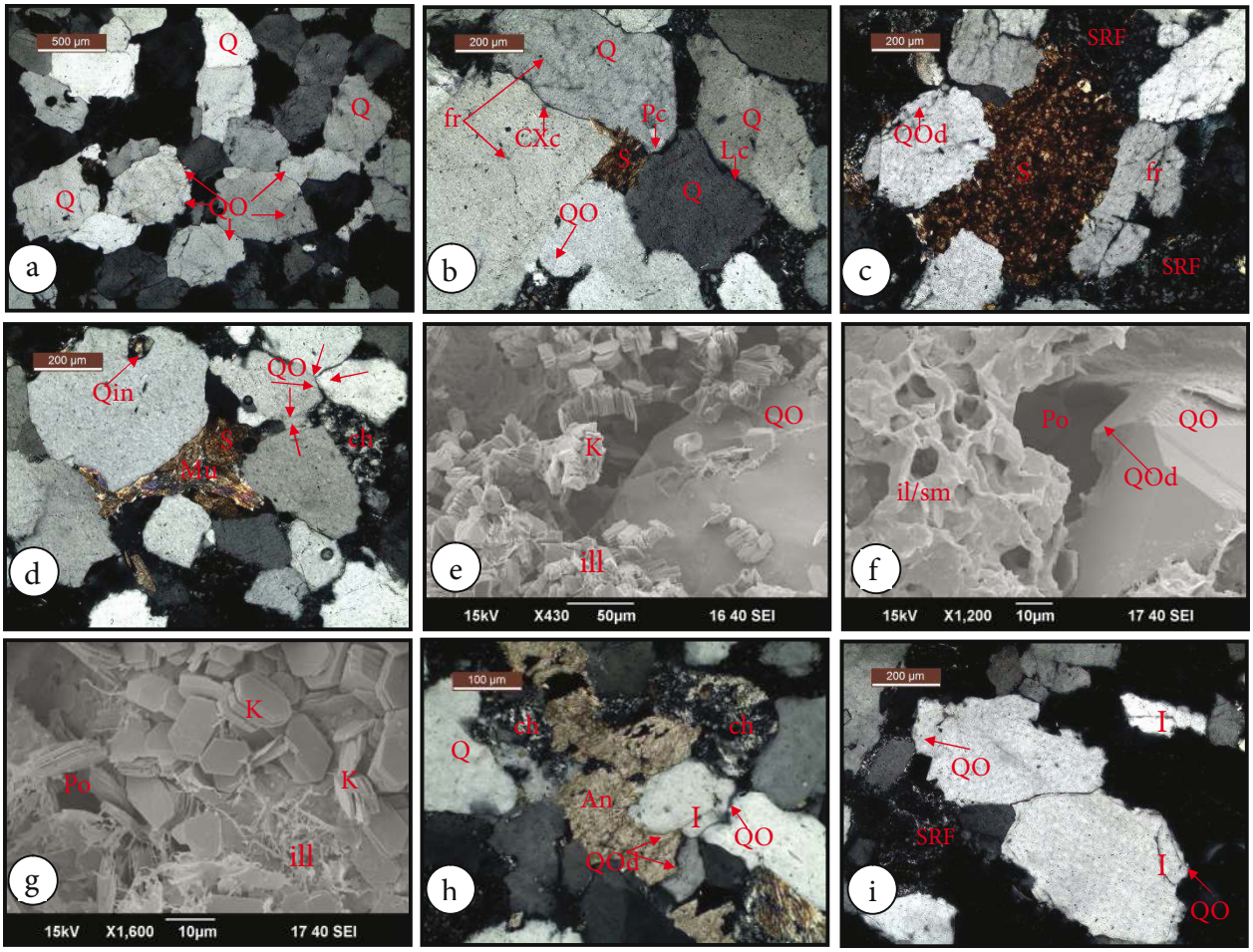

Figure 4. Photomicrographs of Hawkesbury Sandstone showing: **(a)** quartz arenite, where quartz grains (Q) are medium- to coarse-grained, subangular to subrounded, moderately sorted and well cemented with quartz (QO) (note: reduction in primary porosity); **(b)** quartz arenite, with pore-filling siderite cement (S) along the margin of detrital quartz grain (note: point (Pc), long (Lc), concave–convex contact (CXc), and deformation fractures (fr)); **(c)** pore-filling siderite cement (S) filled up the interstitial space between quartz grains (note: fractured quartz grains and dissolution of detrital quartz and authigenic silica (QOd)); **(d)** quartz arenite, where siderite (S) engulfed bent flexible muscovite grains, thus postdating mechanical compaction (note: chert (ch) quartz inclusions (Qin), and double and triple quartz overgrowths (red arrows)); **(e)** quartz arenite, late-phase kaolinite (K), early-phase quartz overgrowth (QO); **(f)** quartz arenite, dissolution of silica overgrowth (QOd) (note: mixed-layer illite/smectite (il/sm) coatings, postdating quartz overgrowth (QO)); **(g)** sublithic arenite, where kaolinite exists as booklets and vermicular aggregates (note: small pore (Po) between authigenic kaolinite, and kaolinite coated by fibrous illite (Il); **(h)** sublithic arenite, with ankerite cement (An) engulfed, thus postdating quartz overgrowth (QO) (note: dust line of iron oxide cement (I) separating detrital quartz (Q) from authigenic silica (QO)); **(i)** sublithic arenite, where quartz overgrowth occurs as pore-filling cement along the margin of detrital quartz grain (note: silica overgrowths engulf, thus postdating iron oxide (I)).

as pore fillings are silica, carbonate (siderite, calcite, dolomite, and ankerite), clays (kaolinite, illite, mixed-layer clay, and chlorite) and iron oxides, with siliceous cement being predominant. A portion of oversized pores (2%) is presumed to be due to the dissolution of feldspars, authigenic silica, and other unstable minerals.

4.2. Clay mineralogy

The clay minerals identified in sandstones are kaolinite, mixed-layer illite/smectite, illite, and chlorite in decreasing order of their abundance. Kaolinite and mixed-layer illite/smectite (avg. 18.35%) dominate over illite and chlorite (avg. 1.4%; Table 2). These variations may be related to relative changes in the climatic conditions in the source area. The moderate crystallinity exhibited by the clay minerals indicates their detrital origin from weathering horizons and soils developed on silicic rocks, and transportation in a fluvial environment (Keller, 1956; Abu-Zeid et al., 1989, 1991). Source area weathering is confirmed by the absence

of smectite and the low percentage of chlorite (Table 2; Figure 4). The predominance of kaolinite with little or no illite indicates their sedimentary origin under continental conditions (Lonnie, 1982; Tsuzuki and Kawabe, 1983; Amer et al., 1989).

4.3. Diagenetic minerals

The most common diagenetic constituents of the Hawkesbury Sandstone are quartz overgrowths, carbonate cements, authigenic clay minerals. and iron oxides.

4.3.1. Authigenic quartz

Authigenic quartz is present in all samples under investigation. It was better developed in large intergranular pore networks and the pores are often occluded by large quartz overgrowths (Figures 4a, 4h, 4i, and 5a–5c). It ranges between 0.5% and 8.5% with an average of 6.18% (Table 2). Quartz cement mainly occurs as syntaxial overgrowths (Figures 4e, 5c, and 5d). It also occurs as syntaxial outgrowths in clay-coat-rich sandstones (Figures 4h, 4i, 5a, and 5e). Thus, quartz overgrowth is recorded as the second cement in this unit after iron oxide. The pore waters required for the precipitation of these overgrowths would have been acidic or slightly alkaline, in an environment containing sufficient dissolved silica to allow quartz overgrowth formation.

During diagenesis, sediments were subjected to different conditions that might activate sources of silica for quartz cementation, such as dissolution of feldspar (Hawkins, 1978), pressure solution (Bjorlykke et al., 1986; Houseknecht, 1988; Dutton and Diggs, 1990; Bjørlykke and Egeberg, 1993; Dutton, 1993; Walderhaug, 1994), replacement of quartz and feldspar by calcite (Burley and Kantorowicz, 1986), and transformation of clay (Hower et al., 1976; Boles and Franks, 1979; Rodrigo and Luiz, 2002). The dissolved silica of the Hawkesbury Sandstone was probably derived from the extensive dissolution of feldspar and volcanic lithic fragments, kaolinitization, and chemical compaction (Zhang et al., 2008; Umar et al., 2011).

4.3.2. Carbonate cement

Carbonate cement is the second cement in the studied sandstones. It ranges from 0% to 35.1%, with an average of 3.89%. The carbonate cement contains siderite, calcite, ankerite, and dolomite. Generally, siderite cement is more common than ankerite, dolomite, and calcite cement phases (Figures 4 and 5).

Siderite ranges between 0.0% and 15.7% with an average of 2.97% (Table 2). It exists as fine- and medium-grained rhombs, as microcrystalline siderite (≤50 μm), and as coarse crystalline siderite (up to 200 μm; Figures 4c and 5f). Siderite is usually stained by iron oxide and contains rare fluid inclusions. It also occurs as pore-filling cement between quartz grains (Figures 4b–4d and 5f) as well as grain coatings (Figure 5g). Siderite cement is observed with quartz grains in most samples where it fills small pores between tightly packed quartz grains.

Ankerite ranges between 0% and 13.2% with an average of 0.55% (Table 2). It is not recorded in most samples. Ankerite cement also fills pore between quartz grains and is present as poikilotopic cement (Figure 4h).

Dolomite (0%–5.4%) is recorded only in a few samples, while trace amounts of calcite (0%–0.8%) are restricted to 4 samples (Table 2). Thus, calcite cement is less prevalent than dolomite cement. Weakly ferroan calcite is the minor carbonate cement phase in the Hawkesbury Sandstone (Figure 5g). It commonly occurs in association with detrital carbonate components, suggesting that these acted as nuclei for cement formation. The ferroan calcite cement has survived dolomitization, most probably due to poor permeability for the circulation of Mg-rich fluids. The source of magnesium is released through the washing of clay minerals. On the other hand, widespread ferroan carbonate cementation is thought to have occurred under reducing alkaline pore water conditions (Morad, 1998; El-ghali et al., 2009). The ions required for cement formation were probably derived from alumino-silicate grain dissolutions and clay mineral transformations.

4.3.3. Authigenic clay minerals

Authigenic clay minerals principally comprise kaolinite, illite, mixed-layer illite/smectite, and chlorite. The authigenic clay minerals form the second-most abundant cement in the Hawkesbury Sandstone, with kaolinite being the most widespread authigenic clay mineral. They fill pores and replace detrital grains and earlier clays (Spry, 2000).

Kaolinite (2.5%–31.8%) is ubiquitous in the Hawkesbury Sandstone. It is present as booklets and vermicular aggregates and occurs in the mud matrix, pseudomatrix, and detrital grains as pore-filling cement (Figures 5d and 5h) and as grain coatings (Figure 4e). Primary and secondary pore spaces are often filled by authigenic kaolinite (Figures 5d and 5h). Kaolinite is present with illite and quartz overgrowths in most samples (Figures 4e and 5d). Quartz overgrowths are enclosed by authigenic kaolinite and this indicates that the latter was precipitated after the quartz overgrowths (Figures 4e and 5d).

The kaolinite formation is dependent on sufficient porosity and permeability to allow migration of interstitial pore waters and to provide growth space, on the presence of K-feldspar and/or muscovite as a source of Al and Si, and on pore waters of an acidic pH.

Mixed-layer illite/smectite (0.2%–17.2%) is the second-most abundant clay mineral in the Hawkesbury Sandstone. Mixed-layer illite/smectite has a honeycomb-like texture. Mixed-layer illite/smectite is observed as pore-lining

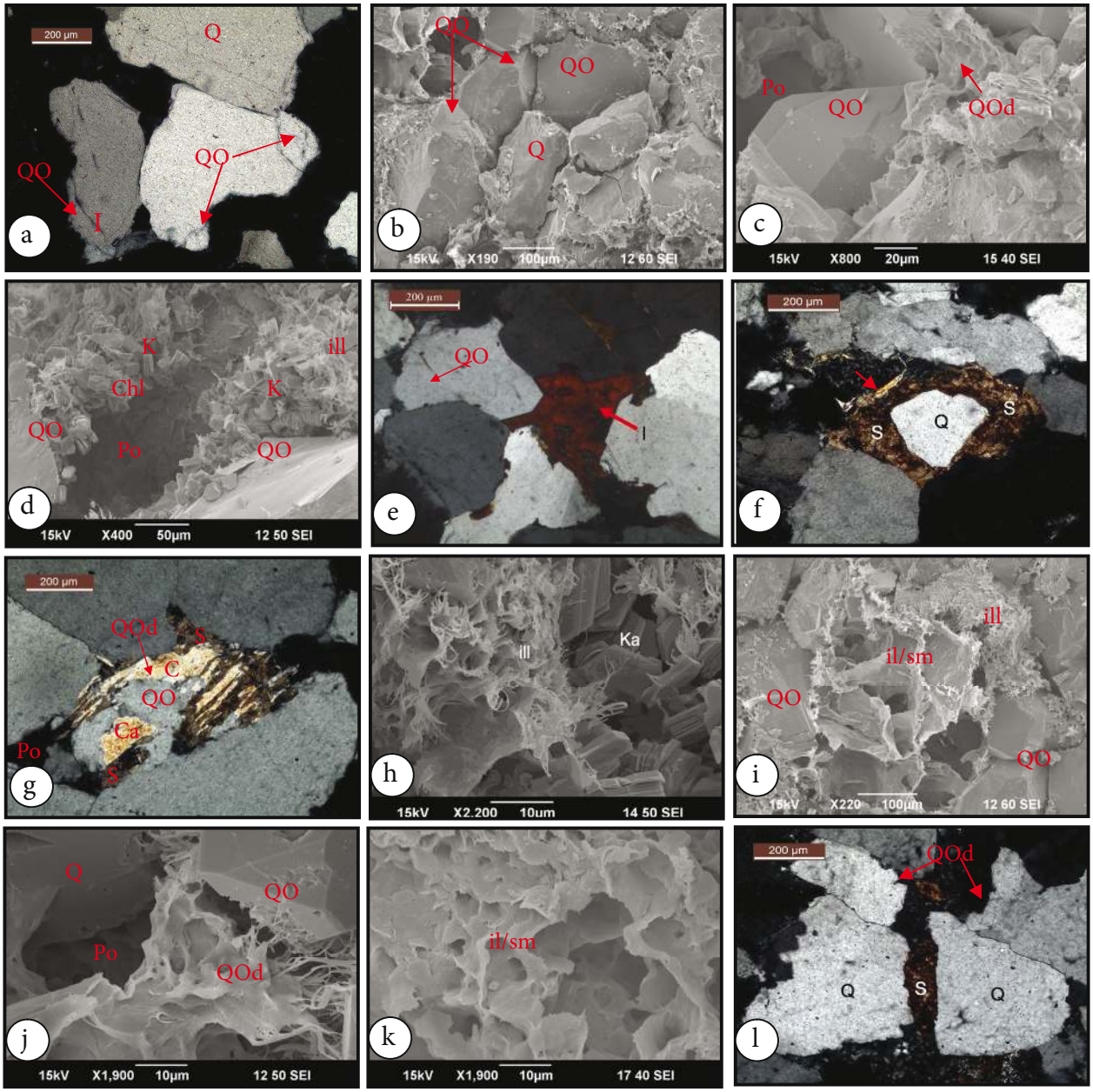

Figure 5. Photomicrographs and SEM images of Hawkesbury Sandstone showing: **(a)** detrital quartz (Q) coated by iron oxide (I) and then engulfed by quartz overgrowth (QO); **(b)** SEM image of early stage of secondary quartz overgrowth (QO); **(c)** SEM image of quartz overgrowth completely filling the intergranular pore (Po) (note: quartz overgrowth dissolution (QOd)); **(d)** SEM image of large pore (Po) coated by kaolinite (K) (note: kaolinite engulfed quartz overgrowths (QO) and chlorite intergrown with authigenic kaolinite); **(e)** pore-filling iron oxide cement engulfed and stained quartz overgrowth (note: silica overgrowth completely fills the interparticle pore); **(f)** quartz grain (Q) is engulfed by siderite cement (S) (note: bent muscovite grain (red arrow)); **(g)** 3 successive cements: quartz overgrowth, calcite, and Fe-calcite cement (siderite) (note: siderite cement grows as cleavage plane around quartz grains and quartz overgrowth dissolution (QOd) by calcite cement (Ca)); **(h)** SEM image of kaolinite booklets (K) engulfed by fibrous illite (ill); **(i)** SEM image of quartz overgrowth (QO) coated by fibrous illite (ill) and mixed-layer clay (ch/sm); **(j)** SEM image of dissolution of authigenic silica (QOd); **(k)** SEM image of mixed-layer clay-illite/smectite (il/sm); **(l)** dissolution of detrital quartz grains (Q) and authigenic silica (QOd) by siderite cement (S).

to pore-filling clay with a ragged-platy morphology. It occurs within quartz overgrowths in some samples. Mixed layer illite/smectite is present as grain coatings and thus postdates the quartz cementation (Figure 4f).

Illite (0%–4.5%) is visible as fibrous illite, mat-like and lath-like crystals within kaolinite, mud matrix, and mud intraclast (Figures 4e, 4g, 5d, 5h, and 5i). It is oriented perpendicular to grain surfaces. Additionally, illite appears as platelets arranged on the framework grain surfaces and as high-birefringence patches. It coats kaolinite and quartz grain edges (Figures 5d and 5h). Illite, which typically forms during progressive burial under elevated temperatures (90–130 °C; Morad et al., 2000), required high K-pore water to achieve illitization in the sandstone.

Chlorite (0%–2.1%) exists in the succession as a pore-filling cement and as grain-coatings on authigenic minerals. It occurs as scattered crystals and as rims on quartz overgrowths, and it is intergrown with authigenic kaolinite (Figure 5d). In some samples, chlorite is also present as a grain-coating on kaolinite.

4.4. Major-element geochemistry

The major-element concentrations of the Hawkesbury Sandstone are given in Table 3 with the ratios between elements. These elements are compared in Table 4 with the average composition of passive margin sandstones (Bhatia, 1983), Amazon big river sands (Potter, 1978), and average arkosic sandstones (Pettijohn, 1963), to be used later for investigating provenance and tectonic setting.

Table 3 shows that most of sandstone samples are rich in SiO_2 (77.6%–95.73%). The source of silica is mainly quartz, chert, quartzite, feldspars, and clay minerals. Sandstones have a wide range of Al_2O_3 (1.19%–3.45%), MgO (0.41%–3.6%), CaO (0.03%–5.3%), K_2O (0.39%–1.2%), and Fe_2O_3 (1.02%–3.9%). Al_2O_3 and K_2O content may be related to the presence of K-feldspars (orthoclase and microcline), illite, and mica, while MgO and CaO content may be related to the presence of carbonate cements and Fe_2O_3 content may be related to the abundance of iron oxide heavy minerals and partly to Fe-containing clay minerals. In contrast, the Hawkesbury Sandstone possesses low average contents of Na_2O, TiO_2, MgO, and CaO. The source of Na_2O is principally related to plagioclase feldspar. Ti-opaque minerals and rutile are the main holders of TiO_2. MgO content is related mostly to the presence of ankerite and dolomite cements. Carbonate cement and diagenesis of plagioclase are the main sources for CaO.

The Hawkesbury Sandstone is highly depleted in most of the major elements except SiO_2 (due to enrichment in quartz and chert), suggesting an intense degree of weathering and reworking that removed ferromagnesian minerals and feldspars. Using the geochemical classification diagram of Herron (1988) and Pettijohn et al. (1972), the Hawkesbury Sandstone is mostly composed of quartz arenites with subordinate sublithic arenites (Figures 6a and 6b), which is consistent with the petrographic data. The depletion of Na_2O content for the Hawkesbury Sandstone (0.27 ± 0.13, n = 32) can be attributed to the relative absence of Na-plagioclase, consistent with the petrographic data. K_2O and Na_2O contents and their ratios (2.93 ± 1.63, n = 32) are also consistent with the petrographic observations, according to common presence of K-feldspar, illite, and muscovite (McLennan et al., 1983; Nath et al., 2000; Zhang, 2004; Osae et al., 2006). Al_2O_3 content is low in Hawkesbury Sandstone (1.81 ± 0.54, n = 32), supporting the minor presence of K-feldspar, clay minerals, and mica. Similarly, generally low concentrations of TiO_2 (0.19 ± 0.04, n = 32) reflect low abundances of Ti-opaque minerals and rutile in the analyzed samples.

On the Al_2O_3/TiO_2 vs. $(SiO_2)_{adj}$ plot of Le Bas et al. (1986) shows that samples of Hawkesbury Sandstone are exclusively felsic in composition (Figure 7). The correlation between SiO_2 and Al_2O_3 is negative for the studied sandstone samples (r = –0.886, n = 32; Table 5), indicating that much of the SiO_2 is present as quartz grains (Akarish and El-Gohary, 2008; Ahmad and Chandra, 2013). A positive correlation between K_2O and Al_2O_3 (r = 0.776) implies that the concentrations of the K-bearing minerals have significant influence on Al distribution and suggests that the abundance of these elements is primarily controlled by the content of clay minerals (McLennan et al., 1983; Jin et al., 2006; Akarish and El-Gohary, 2008). The variations in other major elements of Hawkesbury Sandstone like P_2O_5, MgO, Fe_2O_3, K_2O, Na_2O, and TiO_2 (Table 3) indicate a mixed source rock.

5. Discussion

5.1. Tectonic setting

Dickinson and Suczek (1979) and Dickinson et al. (1983) related detrital sandstone compositions to major provenance types such as stable cratons, basement uplifts, magmatic arcs, and recycled orogens. To interpret the tectonic discrimination source fields, the Hawkesbury Sandstone was plotted on the QtFL and QmFLt ternary diagrams of Dickson et al. (1983). The Hawkesbury sandstone samples are plotted in cratonic interior or recycled orogenic fields (Figures 8a and 8b). Such a craton type reflects mature sandstones derived from relatively low-lying granitoid and gneissic sources, supplemented by recycled sands from associated platform or passive margin basins (Dickson et al., 1983). The low percentage of unstable grains (feldspar and other rock fragments; <8.0%), the dominance of monocrystalline quartz, and the alteration of feldspar grains suggest that the source area underwent a long period of intensive chemical weathering in a warm humid climate (Pettijohn et al., 1987; Amireh, 1991).

Table 3. Major element concentrations (wt.%) of Hawkesbury Sandstone.

Location	Hawkesbury Sandstone																																Statistical parameters		
	S6	S7	S8	S9	S10	S11	S12	EAW1	EAW2	EAW3	EAW4	EAW5	EAW7	EAW8	EAW9	EAW10	EDEN1	EDEN2	EDEN3	EDEN4	EDEN5	EDEN6	EDEN7	EDEN8	EDEN9	EDEN10	EDEN11	EDEN12	EDEN13	EDEN14	EDEN15	EDEN16	n	Mean	SD
$(SiO_2)_{adj}$	94.80	95.22	94.24	93.04	94.65	93.36	95.03	85.07	95.12	88.30	94.32	93.09	94.86	91.28	93.02	94.95	95.57	95.85	94.41	94.90	95.14	94.35	84.99	95.04	95.37	92.62	84.59	91.89	89.66	93.44	93.82	93.76	32.00	92.99	3.13
SiO_2	92.62	92.84	92.26	90.98	92.88	91.81	94.03	80.73	94.53	84.77	92.52	91.60	94.48	87.90	90.60	93.52	95.00	95.73	94.13	94.71	94.95	93.64	77.60	94.16	94.80	90.12	78.75	89.78	83.47	92.13	92.13	91.32	32.00	90.95	4.78
TiO_2	0.22	0.23	0.21	0.22	0.21	0.23	0.22	0.23	0.15	0.21	0.22	0.24	0.21	0.23	0.21	0.19	0.22	0.12	0.19	0.14	0.12	0.14	0.15	0.14	0.16	0.17	0.19	0.16	0.14	0.15	0.14	0.17	32.00	0.19	0.04
Al_2O_3	1.52	1.20	1.80	3.45	1.79	3.17	1.19	2.80	1.40	2.57	1.80	2.02	1.60	1.90	1.84	1.78	1.48	1.35	1.70	1.80	1.80	2.30	1.80	1.67	1.31	1.49	1.83	1.60	1.33	2.20	1.35	1.23	32.00	1.81	0.54
$Fe_2O_3^*$	1.85	1.45	1.90	1.60	1.81	1.76	2.05	2.30	1.45	3.31	1.70	1.56	1.46	1.40	1.30	1.20	1.25	1.02	1.63	1.10	1.02	1.32	3.30	1.30	1.35	1.66	3.90	2.63	2.60	1.60	2.30	1.40	32.00	1.80	0.70
MnO	0.04	0.03	0.01	0.01	0.02	0.01	0.01	0.06	0.01	0.03	0.03	0.02	0.01	0.01	0.01	0.01	0.02	0.01	0.02	0.01	0.01	0.01	0.03	0.02	0.01	0.01	0.01	0.02	0.01	0.01	0.01	0.02	32.00	0.02	0.01
MgO	0.57	0.61	0.54	0.53	0.54	0.53	0.52	3.60	0.68	0.59	0.61	1.10	0.73	1.50	1.07	0.54	0.54	0.51	0.41	0.42	0.41	0.74	1.30	0.61	0.52	0.53	1.50	0.64	0.84	0.52	0.51	0.72	32.00	0.78	0.59
CaO	0.10	0.44	0.25	0.14	0.09	0.16	0.14	4.40	0.30	3.40	0.42	0.80	0.11	2.10	1.26	0.41	0.12	0.03	0.23	0.10	0.10	0.61	5.30	0.50	0.30	2.40	5.30	1.90	3.90	1.30	1.10	2.10	32.00	1.24	1.58
Na_2O	0.23	0.17	0.30	0.24	0.19	0.11	0.19	0.21	0.24	0.30	0.19	0.33	0.32	0.38	0.33	0.26	0.17	0.32	0.44	0.49	0.43	0.09	0.60	0.21	0.31	0.28	0.55	0.30	0.22	0.22	0.08	0.04	32.00	0.27	0.13
K_2O	0.54	0.51	0.62	0.61	0.58	0.55	0.59	0.56	0.61	0.80	0.59	0.72	0.67	0.85	0.76	0.56	0.58	0.77	0.93	1.02	0.95	0.39	1.20	0.45	0.63	0.63	1.06	0.66	0.58	0.46	0.57	0.39	32.00	0.67	0.19
P_2O_5	0.01	0.02	0.01	0.01	0.02	0.01	0.01	0.01	0.01	0.02	0.01	0.01	0.01	0.03	0.02	0.02	0.02	0.01	0.02	0.01	0.01	0.01	0.02	0.01	0.01	0.01	0.01	0.01	0.01	0.01	0.01	0.01	32.00	0.01	0.01
LOI	2.30	2.50	2.10	2.21	1.87	1.66	1.05	5.10	0.62	4.00	1.91	1.60	0.40	3.70	2.60	1.51	0.60	0.13	0.30	0.20	0.20	0.75	8.70	0.93	0.60	2.70	6.90	2.30	6.90	1.40	1.80	2.60	32.00	2.25	2.09
Total	100	100	100	100	100	100	100	100	100	100	100	100	100	100	100	100	100	100	100	100	100	100	100	100	100	100	100	100	100	100	100	100	32.00	100	0.00
CaO*	0.10	0.44	0.25	0.14	0.09	0.16	0.14	4.40	0.30	3.40	0.42	0.80	0.11	2.10	1.26	0.41	0.12	0.03	0.23	0.10	0.10	0.61	5.30	0.50	0.30	2.40	5.30	1.90	3.90	1.30	1.10	2.10	32.00	1.24	1.58
CIA	56.73	42.16	52.38	72.23	61.52	74.55	49.34	23.77	46.39	25.34	50.97	41.92	52.12	26.05	33.33	49.78	56.46	48.48	43.88	45.93	48.09	57.62	13.07	48.76	42.74	21.22	13.49	25.45	14.09	40.44	32.79	22.15	32.00	41.66	16.21
PIA	34.39	22.29	32.38	58.07	39.42	60.21	22.22	18.50	23.98	16.59	32.45	25.36	27.92	13.13	18.07	32.42	31.93	17.82	17.27	17.07	19.95	46.79	3.41	34.19	19.95	11.27	4.83	13.81	7.28	31.07	17.44	14.36	32.00	24.56	13.51
CIW	73.06	52.61	65.48	84.15	78.98	87.03	67.71	25.09	59.80	27.76	62.55	50.25	68.76	29.92	39.33	60.25	74.81	69.91	59.80	64.56	66.93	64.62	14.47	57.07	55.36	23.57	14.77	28.81	15.12	44.63	38.74	24.02	32.00	51.56	21.50
ICV	2.34	2.87	2.13	0.97	1.92	1.06	3.13	4.06	2.46	3.36	2.09	2.36	2.19	3.41	2.68	1.78	1.96	2.06	2.26	1.82	1.69	1.43	6.60	1.93	2.50	3.81	6.84	3.94	6.23	1.94	3.49	3.93	32.00	2.85	1.46
Al_2O_3/TiO_2	6.91	5.22	8.57	15.68	8.52	13.78	5.41	12.17	9.33	12.24	8.18	8.42	7.62	8.26	8.76	9.37	6.73	11.25	8.95	12.86	15.00	16.43	12.00	11.93	8.19	8.76	9.63	10.00	9.50	14.67	9.64	7.24	32.00	10.04	2.90
K_2O/Na_2O	2.35	3.00	2.07	2.54	3.05	5.00	3.11	2.67	2.54	2.67	3.11	2.18	2.09	2.24	2.30	2.15	3.41	2.41	2.11	2.08	2.21	4.33	2.00	2.14	2.03	2.25	1.93	2.20	2.64	2.09	7.13	9.75	32.00	2.93	1.63
SiO_2/Al_2O_3	60.93	77.37	51.26	26.37	51.89	28.96	79.02	28.83	67.52	32.98	51.40	45.35	59.05	46.26	49.24	52.54	64.19	70.91	55.37	52.62	52.75	40.71	43.11	56.38	72.37	60.48	43.03	56.11	62.76	41.88	68.24	74.24	32.00	53.88	14.04
Fe_2O_3/MgO	3.25	2.38	3.52	3.02	3.35	3.32	3.94	0.64	2.13	5.61	2.79	1.42	2.00	0.93	1.21	2.22	2.31	2.00	3.98	2.62	2.49	1.78	2.54	2.13	2.60	3.13	2.60	4.11	3.10	3.08	4.51	1.94	32.00	2.71	1.05
Moles																																			
Al_2O_3	0.015	0.012	0.018	0.034	0.018	0.031	0.012	0.027	0.014	0.025	0.018	0.020	0.016	0.019	0.018	0.017	0.015	0.013	0.017	0.018	0.018	0.023	0.018	0.016	0.013	0.015	0.018	0.016	0.013	0.022	0.013	0.012	32.00	0.018	0.005
CaO	0.002	0.008	0.004	0.003	0.002	0.003	0.003	0.079	0.005	0.061	0.008	0.014	0.002	0.038	0.023	0.007	0.002	0.001	0.004	0.002	0.002	0.011	0.095	0.009	0.005	0.043	0.095	0.034	0.070	0.023	0.020	0.038	32.00	0.022	0.028
Na_2O	0.004	0.003	0.005	0.004	0.003	0.002	0.003	0.003	0.004	0.005	0.003	0.005	0.005	0.006	0.005	0.004	0.003	0.005	0.007	0.008	0.007	0.001	0.010	0.003	0.005	0.005	0.009	0.005	0.004	0.004	0.001	0.001	32.00	0.004	0.002
K_2O	0.006	0.006	0.007	0.007	0.006	0.006	0.006	0.006	0.007	0.009	0.006	0.008	0.007	0.009	0.008	0.006	0.006	0.008	0.010	0.011	0.010	0.004	0.013	0.005	0.007	0.007	0.012	0.007	0.006	0.005	0.006	0.004	32.00	0.007	0.002
P_2O_5	0.000	0.000	0.000	0.000	0.000	0.000	0.000	0.000	0.000	0.000	0.000	0.000	0.000	0.000	0.000	0.000	0.000	0.000	0.000	0.000	0.000	0.000	0.000	0.000	0.000	0.000	0.000	0.000	0.000	0.000	0.000	0.000	0.229	0.000	0.000

n = Number of samples; SD = standard deviation; $(SiO_2)adj$ = major-element data recalculated to anhydrous (LOI-free) basis and adjusted to 100%; $Fe_2O_3^*$ = total Fe expressed as Fe_2O_3. CIA = $[Al_2O_3/(Al_2O_3 + CaO^* + Na_2O + K_2O)] \times 100$; PIA = $[(Al_2O_3-K_2O)/(Al_2O_3 + CaO^* + Na_2O + K_2O)] \times 100$; CIW = $[Al_2O_3/(Al_2O_3 + CaO^* + Na_2O)] \times 100$ (Nesbitt and Young, 1982). CaO^* = CaO in silicate phase. To calculate CaO*, the assumption proposed by McLennan et al. (1993) was followed. ICV = $(Fe_2O_3 + K_2O + Na_2O + CaO + MgO + MnO + TiO_2)/Al_2O_3$ (Cox et al., 1995).

Table 4. Comparison of the average chemical compositions of the studied Middle Triassic Hawkesbury Sandstone and other different sandstones.

	Modern big rivers (Amazon) (Potter, 1978)	Arkose (Pettijohn, 1963)	Passive margin (Bhatia, 1983)	Present work
SiO_2	85.32	80.18	81.95	90.95
Al_2O_3	7.47	9.04	8.41	1.81
TiO_2	0.78	0.31	0.49	0.19
Fe_2O_3	2.76	2.37	3.28	1.80
MnO	0.05	0.28	0.05	0.02
CaO	1.12	2.81	1.89	1.24
MgO	1.02	0.52	1.39	0.78
Na_2O	0.23	1.56	1.07	0.27
K_2O	1.14	2.91	1.71	0.67
P_2O_5	0.02	0.10	0.12	0.01
K_2O/Na_2O	5.00	1.86	1.60	2.93
Fe_2O_3/MgO	3.78	2.89	2.89	2.71
Al_2O_3/SiO_2	0.09	0.11	0.10	0.02

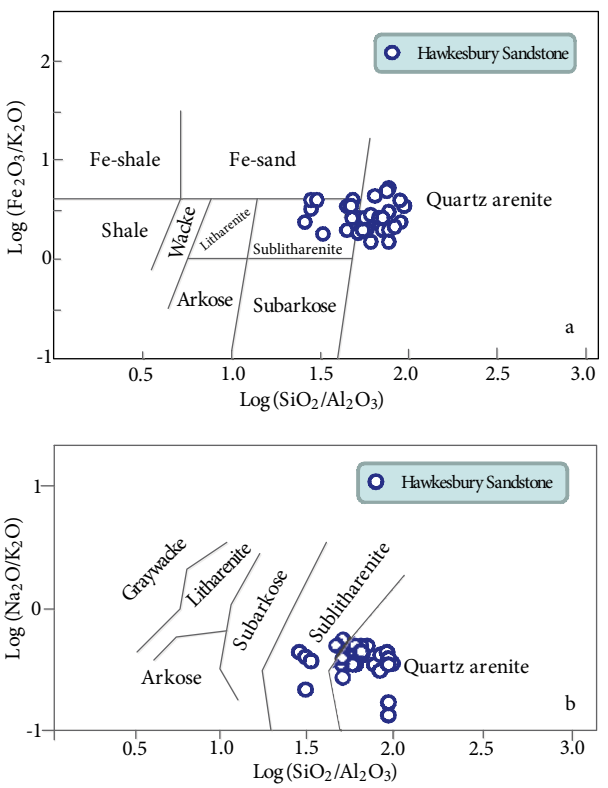

Figure 6. Chemical classification of the Hawkesbury Sandstone based on **(a)** the log (SiO_2/Al_2O_3) vs. log (Fe_2O_3/K_2O) diagram of Herron (1988) and **(b)** the log (SiO_2/Al_2O_3) vs. log (Na_2O/K_2O) diagram of Pettijohn et al. (1972).

The percentage of major elements (Table 3) was used to discriminate the tectonic setting of sandstones (Schwab, 1975; Bhatia, 1983; Roser and Korsch 1986, 1988; Armstrong-Altrin et al., 2004). The discriminant function diagrams were used to understand the provenance for the Hawkesbury Sandstone. The discriminant function diagram of Roser and Korsch (1988) suggests that Hawkesbury Sandstone may be derived exclusively from mature polycyclic continental sedimentary rocks (Figure 9a). The discriminate degrees of Bhatia (1983) favor a passive margin setting for the Hawkesbury Sandstone (Figure 9b). Tectonic discrimination diagrams of Roser

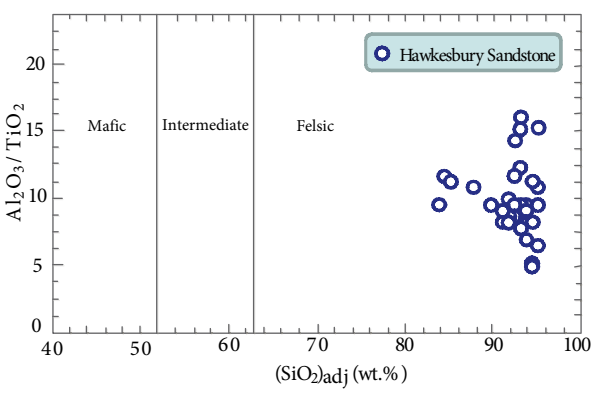

Figure 7. The Al_2O_3/TiO_2 vs. $(SiO_2)_{adj}$ relationship for the Hawkesbury Sandstone (Le Bas et al., 1986).

Table 5. Values of Pearson's coefficient of correlation of major elements of the Hawkesbury Sandstone.

	SiO_2adj	SiO_2	TiO_2	Al_2O_3	Fe_2O_3	MnO	MgO	CaO	Na_2O	K_2O	P_2O_5	LOI	CIA	PIA	CIW
SiO2adj	1														
SiO_2	0.981*	1													
TiO_2	−0.064	−0.085	1												
Al_2O_3	−0.906	−0.886	0.206	1											
Fe_2O_3	−0.612	−0.649	0.010	0.066	1										
MnO	−0.316	−0.346	0.398	0.116	0.213	1									
MgO	−0.576	−0.574	0.241	0.239	0.258	0.651*	1								
CaO	−0.849	−0.904	−0.061	0.272	0.686*	0.333	0.598*	1							
Na_2O	−0.801	−0.725	−0.199	0.797*	0.352	−0.071	0.187	0.543*	1						
K_2O	−0.797	−0.730	−0.240	0.776*	0.375	−0.022	0.154	0.551*	0.976*	1					
P_2O_5	−0.296	−0.278	0.346	0.479	0.006	0.127	0.045	0.117	0.206	0.208	1				
LOI	−0.829	−0.920	0.080	0.362	0.656*	0.328	0.500*	0.912*	0.500*	0.530*	0.194	1			
CIA	0.251	0.316	0.472	0.372	−0.453	−0.048	−0.264	−0.646	−0.106	−0.113	0.143	−0.417	1		
PIA	0.232	0.286	0.524*	0.377	−0.424	−0.014	−0.229	−0.611	−0.144	−0.153	0.148	−0.374	0.994*	1	
CIW	0.262	0.330	0.444	0.364	−0.467	−0.062	−0.277	−0.659	−0.093	−0.099	0.135	−0.437	0.998*	0.986*	1
ICV	−0.052	−0.173	−0.347	−0.456	0.450	−0.017	0.101	0.500*	−0.216	−0.204	−0.234	0.388	−0.764	−0.722	−0.774

*: Correlation is significant at the 0.05 level (2-tailed).

and Korsch (1986) suggest that the Hawkesbury Sandstone falls exclusively in the field of passive tectonic margin (Figure 9c). In such a setting, the sediments are largely quartz-rich sandstones that derived from plate interior or stable continental areas and were deposited in the intracratonic basin or passive continental margins (Roser and Korsch, 1986).

In silica-rich sands (SiO_2 > 70%) with a K_2O/Na_2O ratio of more than unity (Bhatia, 1983) and FeO + MgO content of less than 5% (Taylor and McLennan, 1985), the correlation with a passive margin setting is distinct. The Hawkesbury Sandstone meets all of these parameters (Table 3). The uniform chemical characteristics of Hawkesbury Sandstone (e.g., high SiO_2/Al_2O_3, K_2O/Na_2O; Table 3) suggest that it derived from old upper continental crust (McLennan et al., 1990). According to McLennan et al. (1990), this provenance component constitutes old stable cratons and old continental foundations of active tectonic settings.

The tectonic discrimination diagrams proposed by Bhatia (1983) and Roser and Korsch (1986, 1988) have mostly been used to identify the tectonic setting of unknown basins (Jafarzadeh et al., 2013; Nowrouzi et al., 2013). Armstrong-Altrin and Verma (2005) evaluated these major-element-based discrimination diagrams using Miocene to Recent sediments and showed a low percentage success rate (0%–23%) for the Bhatia (1983) diagram and success of 31.5%–52.3% for the diagram of Roser and Korsch (1986, 1988).

Recently, Verma and Armstrong-Altrin (2013) proposed 2 new discriminant-function-based major-element diagrams for the tectonic discrimination of siliciclastic sediments from 3 main tectonic settings: island or continental arc, continental rift, and collision, created for the tectonic discrimination of high-silica [$(SiO_2)_{adj}$ = 63%–95%] and low-silica [$(SiO_2)_{adj}$ = 35%–63%] rocks. The high-silica discriminant-function-based major-element diagram is used in this study to identify the tectonic environment of the studied Hawkesbury Sandstone samples (Table 3). This tectonic discriminant diagram (Verma and Armstrong-Altrin, 2013) suggests that the Hawkesbury Sandstone plots near the line that separates collision and rift fields (Figure 10). The results obtained from this discriminant-function-based multidimensional diagram provides good evidence for the source area tectonic system, which is consistent with the general geology of Hawkesbury Sandstone in the Sydney Basin (Dehghani, 1994; Veevers et al., 1994).

5.2. Source area weathering

The weathering history of ancient sedimentary rocks can be evaluated in part by examining relationships among the alkali and alkaline earth elements (Nesbitt and Young, 1982). A good measure of the degree of chemical weathering can be obtained by calculation of the chemical

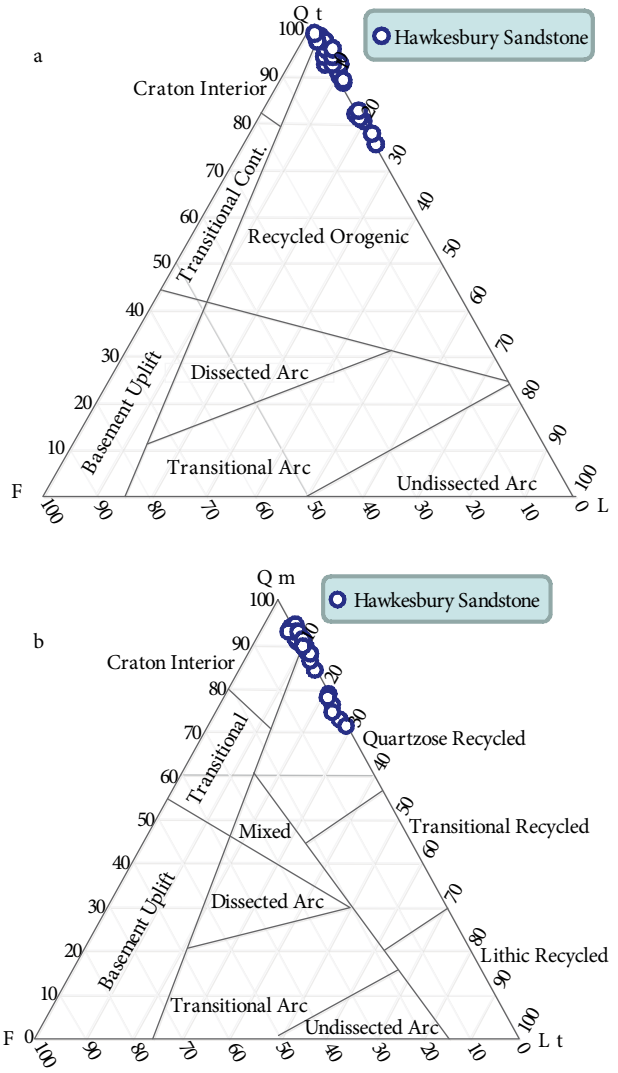

Figure 8. QtFL **(a)** and QmFLt **(b)** ternary diagrams for the Hawkesbury Sandstone, after Dickson et al. (1983).

index of alteration (CIA), plagioclase index of alteration (PIA), and chemical index of weathering (CIW) (Nesbitt and Young, 1982; Fedo et al., 1995). High CIA, PIA, and CIW values (i.e. 75–100) indicate intensive weathering in the source area, whereas low values (i.e. 60 or less) indicate low weathering in the source area. The calculated CIA, PIA, and CIW values for the Hawkesbury Sandstone (Table 3) range from 13.07 to 74.55, with an average of 41.66; from 3.41 to 60.21, with an average of 24.56; and from 14.47 to 87.03, with an average of 51.56 (Table 3), respectively. These values indicate low-moderate to high degrees of weathering, either of the original source or during transport before deposition, and may reflect intense recycling in arid/semiarid climate conditions in the source area (McLennan et al., 1993; Osea et al., 2006). The low CIA values of Hawkesbury Sandstone are due to direct input of immature continent detrital minerals into the depositional system (Bakkiaraj et al., 2010).

The variation in CIA values (n = 32, mean = 41.66, SD = 16.21; median = 44.9) may reflect changes in the proportion of feldspars and the various clay minerals in the analyzed samples. Size sorting during transportation and deposition generally results in some degree of mineral differentiation, which may modify the CIA (Pettijohn, 1975; Nesbit and Young, 1982).

Petrographic evidence such as heterogeneous roundness for different grains (coarser ones are rounded and finer ones are angular) implies the importance of mechanical effects for grain shape configuration. Coarse-grained feldspars are related to a low degree of chemical weathering. Moreover, the rounded quartz overgrowths indicate recycling, which, in turn, can modify the compositional data towards the quartz-rich sandstones. The point count data for the Hawkesbury Sandstone samples on the diagram of Weltje et al. (1998) plot in the metamorphic/sedimentary field and field number 4 (Figure 11a), which indicates that recycling and sedimentation occur in low-relief and tropical humid climatic conditions. According to Laird (1972), the sediments plotted in such fields are mainly derived from deeply weathered granitic-gneissic terrain, which are quartz-rich sandstones, poor in feldspar and rock fragments.

The QFR_F ternary diagram of Suttner et al. (1981) indicates a metamorphic source rock in a humid climate (Figure 11b). However, this particular diagram can discriminate only sources of metamorphic and plutonic rocks (humid or arid conditions), and it does not discriminate between different tectonic settings. The diagrams (Figures 11a and 11b) are defined for first-cycle sediments, and the effect of recycling and long-distance transportation can shift the data on these diagrams toward humid conditions (Jafarzadeh and Hosseini Barzi, 2008). These considerations probably imply that new diagrams should be proposed, such as those suggested in the field of sedimentary rock geochemistry (Armstrong-Altrin and Verma, 2005) and those already proposed in the area of igneous rock geochemistry (e.g., Agrawal et al., 2004; Verma et al., 2006).

To make use of the chemical parameters, the ratio of SiO_2/Al_2O_3 against that of quartz, quartzite, and chert/(feldspar + rock fragments), (Q/F+RF) was plotted (Figure 12a), which is interpreted to reflect the maturity of sandstones (Pettijohn, 1975). A higher SiO_2 ratio coincides with higher silica phases of quartz, quartzite, and chert, which in turn reflect that such sandstones are mature. A bivariate plot of SiO_2 against total $Al_2O_3+K_2O+Na_2O$ as proposed by Suttner and Dutta (1986) was used in order to identify the maturity of the Hawkesbury Sandstone as a

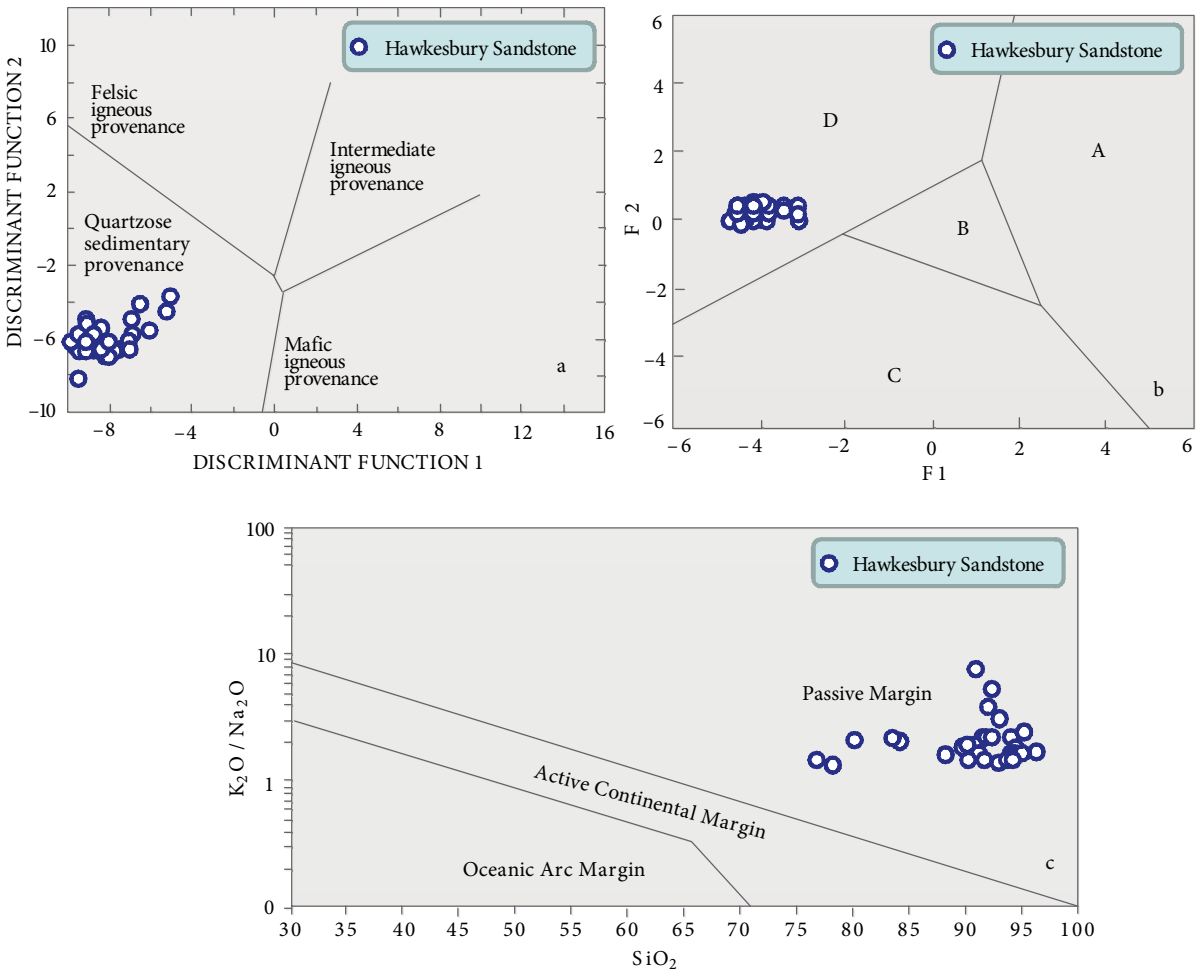

Figure 9. The tectonic discriminant function diagrams for the Hawkesbury Sandstone: **(a)** Roser and Korsch (1988), **(b)** Roser and Korsch (1986). A: Oceanic island arc, B: continental island arc, C: active continental margin, D: passive margin, and **(c)** Bhatia (1983).

function of climate (Figure 12b). This plot revealed humid climatic conditions for the samples investigated.

Paleoweathering conditions can also be detected using the Al_2O_3 -CaO+Na_2O- K_2O (A-CN-K) ternary diagram of Nesbitt and Young (1984) (Figure 13), where unweathered rocks are clustered along the left-hand side of the K-feldspar-plagioclase join (Nesbitt and Young, 1984; Holail and Moghazi, 1998). All the samples analyzed here plot parallel to the A-CN line (Figure 13), defining a nonsteady-state weathering trend towards the "CN" apex, which is probably due to the presence of diagenetic calcite cement rather than Na-rich feldspar. This nonsteady-state weathering indicates balanced rates of chemical weathering and erosion, which produces compositionally similar sediments over a long period (Nesbitt et al., 1997; Selvaraj and Chen, 2006). The result supports the conclusion that the sandstones of the Hawkesbury Sandstone Formation were derived from granitic to granodiorite source terrain (Figure 13). Some samples of the Hawkesbury Sandstone Formation plot close to the Al_2O_3–K_2O boundary, indicating moderate to intense weathering conditions in the source area. Obviously, the highest degree of alteration (in terms of CIA) is compatible with the sediments having maximum kaolinite and less feldspar content. CIA values correlated well with kaolinite content (Table 3). They decrease upwards with a decrease in kaolinite and an increase in feldspar.

5.3. Hydraulic sorting

Hydraulic sorting of detrital mineral grains can significantly influence the chemical composition of bulk sediments. Geochemical variability due to hydraulic sorting can be evaluated using the index of compositional variability (ICV) (Cox et al., 1995). Rock-forming minerals such as plagioclase, k-feldspars, amphiboles, and pyroxenes show ICV values of >0.84, whereas typical alteration products such as kaolinite, illite, and muscovite show values of <0.84

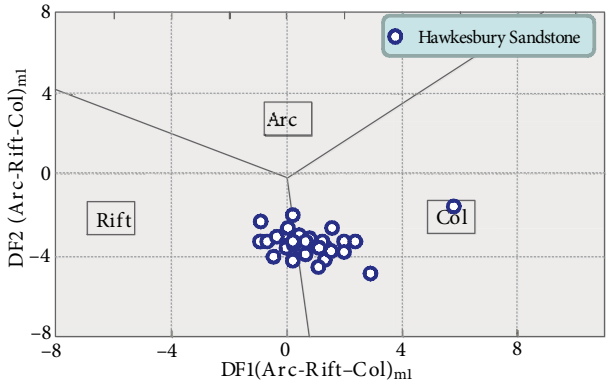

Figure 10. New discriminant-function multidimensional diagram proposed by Verma and Armstrong-Altrin (2013) for high-silica clastic sediments from 3 tectonic settings (arc, continental rift, and collision). The subscript $_{m1}$ in DF1 and DF2 represents the high-silica diagram based on $\log_e$ ratios of major elements. The discriminant function equations are as follows: $DF1_{(Arc\text{-}Rift\text{-}Col)m1} = (-0.263 \times \ln(TiO_2/SiO_2)_{adj}) + (0.604 \times \ln (Al_2O_3/SiO_2)_{adj}) + (-1.725 \times \ln(Fe_2O_3^t/SiO_2)_{adj}) + (0.660 \times \ln(MnO/SiO_2)_{adj}) + (2.191 \times \ln(MgO/SiO_2)_{adj}) + (0.144 \times \ln(CaO/SiO_2)_{adj}) + (-1.304 \times \ln(Na_2O/SiO_2)_{adj}) + (0.054 \times \ln(K_2O/SiO_2)_{adj}) + (-0.330 \times \ln(P_2O_5/SiO_2)_{adj}) + 1.588$. $DF2_{(Arc\text{-}Rift\text{-}Col)m1} = (-1.196 \times \ln(TiO_2/SiO_2)_{adj}) + (1.604 \times \ln (Al_2O_3/SiO_2)_{adj}) + (0.303 \times \ln(Fe_2O_3^t/SiO_2)_{adj}) + (0.436 \times \ln(MnO/SiO_2)_{adj}) + (0.838 \times \ln(MgO/SiO_2)_{adj}) + (-0.407 \times \ln(CaO/SiO_2)_{adj}) + (1.021 \times \ln(Na_2O/SiO_2)_{adj}) + (-1.706 \times \ln(K_2O/SiO_2)_{adj}) + (-0.126 \times \ln(P_2O_5/SiO_2)_{adj}) - 1.068$.

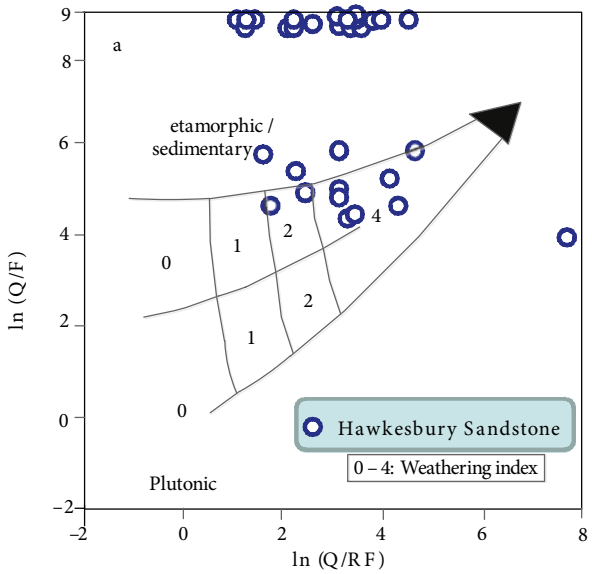

Semiquantitative Weathering Index			Relief		
			High mountain 0	Moderate hills 1	Low plains 2
Climate	Semiarid and Mediterranean	0	0	0	0
	Temperate subhumid	1	0	1	2
	Tropical humid	2	0	2	4

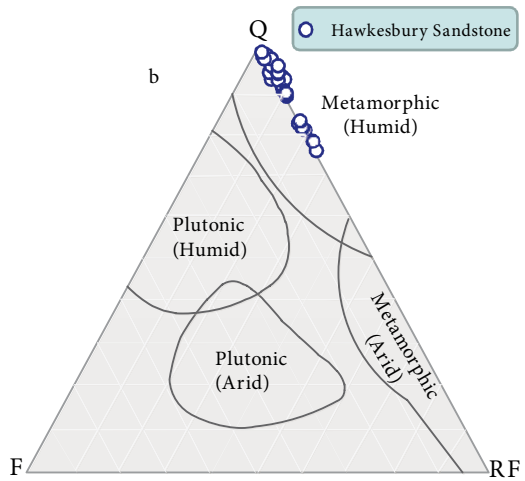

Figure 11. (a) Log-ratio plot after Weltje et al. (1998). Q: Quartz, F: feldspar, RF: rock fragments. Fields 1–4 refer to the semiquantitative weathering indices defined on the basis of relief and climate as indicated in the table. **(b)** The effect of source rock on the composition of the Hawkesbury Sandstone using the diagram of Suttner et al. (1981).

(Cox et al., 1995; Cullers, 2000). The mean ICV values of the Hawkesbury Sandstone (2.85 ± 1.46, n = 32) are higher than 0.84, indicating that they are enriched in rock-forming minerals (Table 3). Similarly, the high SiO_2/Al_2O_3 ratio of the Hawkesbury Sandstone (avg. 53.88) indicates compositionally matured sediments (e.g., Ahmad and Chandra, 2013) (Table 3). This result supported the idea that Hawkesbury sandstones have a recycled orogenic source and are derived mainly from quartzose recycled rocks and/or highly weathered granitic-gneissic rocks (Figures 8 and 9a).

5.4. Provenance

A high percentage of quartz (75.79%–98.81%) and textural features such as coarse-medium to fine grains, moderately good sorting, and the subrounded to rounded shape and low percentage of feldspar (0%–2.16%), and other rock fragments (0%–24.2%) (Tables 1 and 2) show transportation from distant/remote sources or extensive reworking of the sediments and indicate a cratonic or a recycled source for the Middle Triassic Hawkesbury Sandstone (Al-Habri and Khan, 2008). Hawkesbury Sandstone, deposited in the craton interior to recycled orogeny (Figures 8a and 8b), is derived from the exposed basement shield area, probably platform or uplifted basement rocks. They might be derived mainly from weathered and low-lying crystalline basement rocks or from recycled sediments. The Hawkesbury Sandstone

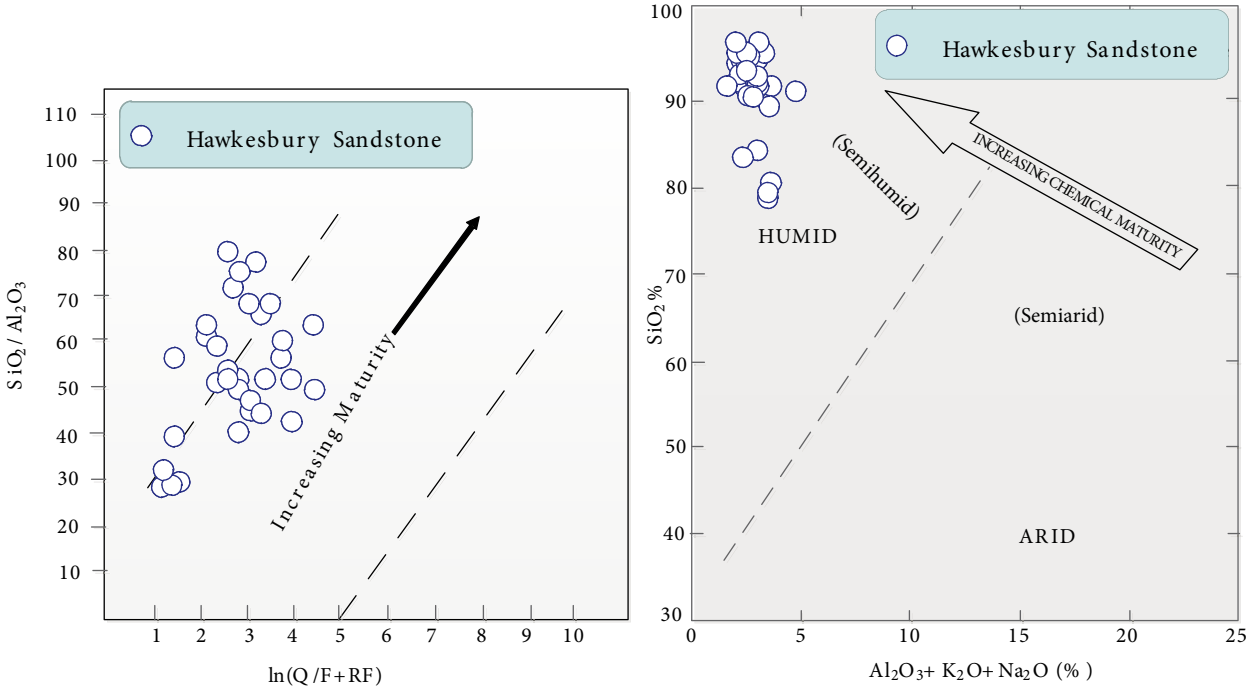

Figure 12. (a) The ratio SiO_2/Al_2O_3 and ln(Q/(F+RF) in the different types of the Hawkesbury Sandstone. **(b)** Chemical maturity of the Hawkesbury Sandstone expressed by bivariate plot of SiO_2 versus Al_2O_3+ K_2O + Na_2O; fields after Suttner and Dutta (1986).

appears to have been deposited mainly by a large-scale braided river system (the Hawkesbury River) flowing from the southwest cratonic Lachlan Fold belt source (Standard, 1969; Veevers, 1984). The presence of mixed altered and fresh feldspars may reflect immature sediments interfingered with more mature phases. This would favor a weathered crystalline granitic source terrain (Pettijohn, 1975; Roser et al., 1996; Akarish and El-Gohary, 2008).

Relatively unstrained monocrystalline quartz grains that contain common inclusions are present in all samples, suggesting a plutonic origin (Basu et al., 1975; Potter, 1978; Hindrix, 2000). The polycrystalline quartz grains composed of 3 or more crystals with straight to slightly curved intercrystalline boundaries indicate that the Hawkesbury Sandstone Formation was derived from plutonic igneous rocks (Folk, 1974; Blatt et al., 1980). The scarcity of feldspar and low percentage of rock fragments or their absence in many samples favors a cratonic source, mature transport regime, and long moderate chemical weathering in a warm, dry climate (Amireh, 1991; Al-Habri and Khan, 2008). The low sedimentary rock fragments and the coaxial crystal overgrowth (i.e. double, triple overgrowth) on quartz grains (Figure 4d) indicate several phases of recycling from older sedimentary sources (Al-Habri and Khan, 2008).

The quantitative petrography provides important information on the nature of the source area. The high proportion of quartz and the dominance of K-feldspar over the more chemically unstable plagioclase in the Hawkesbury Sandstone Formation suggests that the source was exposed to prolonged weathering and that the sediment is at least partially multicyclic (Osae et al., 2006). This mineralogy is consistent with derivation from

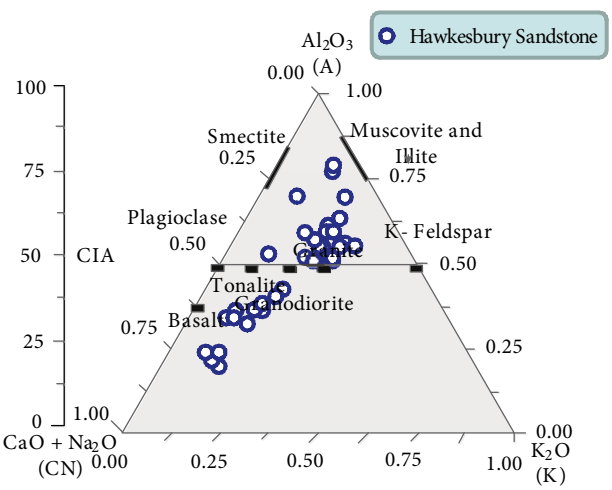

Figure 13. A–CN–K ternary diagram of molecular proportions of Al_2O_3- (CaO^*+Na_2O) – K_2O for the Hawkesbury Sandstone (after Nesbitt and Young, 1984).

plutonic rocks. However, the presence of rare rounded detrital quartz grains, sedimentary lithic fragments, and rounded grains of zircon and tourmaline suggests that a component of the provenance is older (preexisting) sedimentary rocks.

Moreover, the presence of greater than 77% SiO_2 implies that the sandstones are rich in quartz from a quartz-rich crystalline provenance. The K_2O/Na_2O ratio can be considered as a simplified chemical provenance indicator (Potter, 1978). High values of this ratio reflect derivation from granites rather than from basic rocks. This is also confirmed by the clay mineral content, as illite and kaolinite were considered to be inherited from weathering horizons and soils developed on silicic (granitic) rocks. In addition, the absence of smectite and the low percentage of chlorite clay minerals (avg. 0.19%) also preclude mafic source rocks.

Application of cluster analyses of major oxides with their chemical index variations gives good evidence for the tectonic setting and leads to the definition of 2 main clusters (Figure 14a) that could be related to 2 provinces. The mineralogical pattern (Figure 14b) supports the results of the cluster analysis that distinguished 2 mineralogical provinces. The chemical indexes (CIA, PIA,

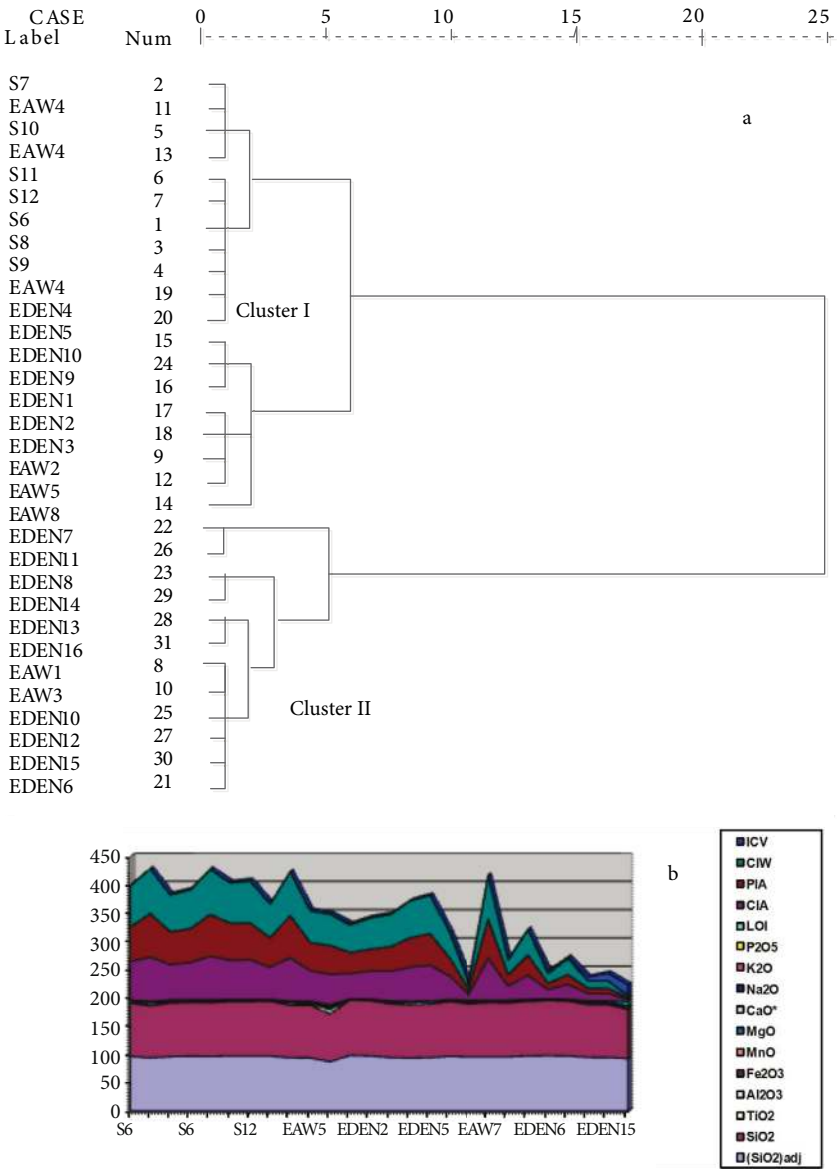

Figure 14. Cluster analysis **(a)** and mineralogical pattern **(b)** of major oxides with their chemical indexes for Hawkesbury Sandstone.

and CIW) also differ in the 2 provinces. This variation suggests the differential effects by hydraulic fractionation and indicates a mixed source. The relatively high values of ultrastable minerals in these provinces is probably due to the large distance of transport and the abundance of clastic sediments in the hinterland as well as the effect of physical marine processes such as waves and currents along the coastal area.

The major-element-based provenance discriminant function diagram of Roser and Korsch (1988) is frequently used by many researchers to identify the provenance of terrigenous sediments (Hofer et al., 2013; Khanchuk et al., 2013; Vdačný et al., 2013) and to reflect the source rock composition (Shadan and Hosseini-Barzi, 2013). This discriminant function diagram reveals that the source sediments of the Hawkesbury Sandstone were mature polycyclic continental sedimentary rocks, supporting the interpretation that they were derived from a granitic-gneissic or sedimentary source area (Figure 9a), and similar to a passive margin-derived source (Roser and Korsch, 1986; Bhatia, 1983). The collective petrographic and geochemical data strongly suggest that the Hawkesbury Sandstone derived from plate interiors or stable continental areas and was deposited in a passive margin of a syn-rift basin.

The coexistence of quartz arenites with subordinate sublithic arenites was interpreted as an interplay of pulses of rapid uplift of the source area and quick subsidence of the basin, followed by a period of quiescence within an overall transgressive-regressive cycle in a rift tectonic regime. During quiescence, the first-cycle quartz sand may have been supplied from a nearby quartz-rich source area. A unique combination of tropical climate, low relief, low rate of sedimentation, and long residence on the beach formed the mature, first-cycle quartz arenites (Suttner et al., 1981). However, the imprint of climate, although preserved for the first 75 km of transportation in high-gradient streams, is rapidly destroyed as soon as a high-energy marine environment (beach) is reached (Suttner et al., 1981). The relative proportion of quartz (92.1%) to feldspars (0.31%) and lithic fragments (7.59%) in the present study's sediments is dependent not only on the source rock and climate, but also to some extent on the degree of stability of the basin of deposition (Dickinson and Suczek, 1979). During basin instability, sediments supplied from the source area were quickly buried and more or less retained the original composition, except for modification of unstable constituents (lithic fragments and feldspars) induced by chemical weathering, which has a greater capacity to alter sandstone composition (Basu, 1976; James et al., 1981; Franzinelli and Potter, 1983; Suttner and Dutta, 1986; Dutta, 1987).

The above-mentioned observations reveal that the Hawkesbury Sandstone may have been derived from a variety of source rocks (mixed provenance). This interpretation is also supported by the presence of abundant opaque mineral grains including iron oxides (hematite), which reflect derivation from metamorphic and igneous rocks. The presence of alkali feldspars indicates their source as plutonic and metamorphic rocks (Trevena and Nash, 1981). The suite of heavy minerals including zircon, rutile, and tourmaline indicates an acid igneous source for these sandstones, while the presence of rounded grains of rutile and zircon is an indication of the reworked source for these sandstones.

Finally, the Proterozoic granites and Permian-Triassic Illawarra Coal Measures and Narrabeen Group could have been the source rocks for Hawkesbury sandstones, which have been uplifted, tilted, and exposed because of the stress built up by the Permian-Triassic rifting. The present study can be used to show that the Proterozoic granitic and Permian-Triassic rocks (i.e. Lachlan and New England Fold Belts) in the southern and northern parts of the Sydney Basin, Australia, were already exposed in Triassic times and supplied sediments by the Hawkesbury River towards the basin.

5.5. Diagenesis

The major diagenetic aspects observed in the Hawkesbury Sandstone are: 1) compaction; 2) iron-oxide cementation; 3) silica cementation; 4) kaolinite and mixed-layer clay cementation; 5) silica dissolution, carbonate cementation, and grain replacement; 6) illite and chlorite authigenesis; and 7) carbonate dissolution and iron-oxide cementation.

5.5.1. Compaction

Sandstones are subjected to mechanical and chemical compactions during their progressive burial, as evidenced from the close packing of the detrital framework, which has caused a reduction in primary porosity of the sandstones (Figure 4a). This compaction is represented by bent flexible muscovite grains (Figures 4d and 5f) and evidenced by concave–convex, sutured contacts of neighboring clastic grains (Figure 4b) and a certain degree of stylolitization. The occurrence of chemical compaction is clear along detrital quartz grains. In other cases, framework grains constitute about 70% of the rock and are embedded in a siliciclastic–carbonate matrix. This primary pore-filling matrix appears to have influenced mechanical compaction and cementation, as evidenced by the presence of fractured and strained detrital quartz grains floating in carbonate cement (Figures 4b and 4c). Hawkesbury Sandstone was subjected to some mechanical compaction until carbonate cementation occurred, which ended the effect of mechanical compaction. However, mechanical compaction continued in sandstones with few carbonates, as indicated by their sutured and long-grain contacts (Umar et al., 2011).

Chemical compaction occurred by pressure dissolution, both along intergranular contacts and fractures (Zhang et

al., 2008). Dissolution of unstable grains (feldspar and rock fragments) is well recorded in some sandstone samples. This dissolution is due to relatively acidic conditions, in which the stability of feldspars is reduced. Dissolution appears to postdate the compaction. This process caused a local increase in porosity.

5.5.2. Iron-oxide cementation

Iron- oxide occurs as a coating around detrital grains (Figures 4h, 4i, and 5a) in Hawkesbury Sandstone. It predated other diagenetic events, such as silica cementation. The iron-oxide minerals are of diagenetic origin, not an oxidized rim of detrital grains, as evidenced by the absence or weak coating of iron oxide at grain contacts. They also fill fractures in detrital quartz, indicating a postcompactional process.

5.5.3. Silica cementation

Silica cement in Hawkesbury Sandstone is mostly quartz overgrowth (Figures 4a, 4b, 4d, 4h, 5a, 5c, 5i, and 5j). In noncalcareous sandstones, development of quartz overgrowth is noticeable, ranging from 5.8% to 8.5%, whereas calcareous sandstones of the transgressive facies yield little quartz overgrowth (less than 3%). The shape of the original grain is delineated by thin dark brown iron coatings developed between the overgrowth and the grain. Silica overgrowth also partially fills the interparticle pore spaces.

Detrital quartz grains are dominated by syntaxial overgrowths (Figures 5c and 5d), probably due to their relatively higher permeability and ease of percolation of water and silica-rich fluids (Al-Habri and Khan, 2008). Silica cement may derive from dissolution of quartz grains, replacement of feldspar, and alteration of clay minerals.

Quartz grains show straight-line boundaries and triple junctions (Figure 4c). These signatures are related to intermediate burial, tectonic uplift and folding of the strata (Ahmed and Baht, 2006). Grain-to-grain boundaries observed in this study appear to have culminated into triple junctions. This culmination evolved through different stages of diagenesis. Taylor (1950) concluded that in the case of point contacts, 2 processes are in operation: solid flow and solution, and redeposition (interstitial transport of dissolved material). With increasing intensity of diagenesis, imposition of self-boundaries between the 2 adjacent grains in close optical orientation gives rise to a compound grain (Figure 4a) (Dapples, 1979). Compound grains consisting of 4 or 5 grains constitute a composite or a cluster (Aalto, 1972) and display uniform optical orientation. Under deep burial conditions, increase in temperature and pressure causes annealing of the grains and facilitates solution and recrystallization in the quartz grains in pure-quartz sandstones. Mobility of constituent chemical components leads to the formation of straight-line boundaries. The precipitation of secondary silica was accompanied by, and most probably succeeded by, partial or complete dissolution of the carbonate fragments.

5.5.4. Kaolinite cementation

Clays represent an average 19.74% of the total cement and appear to derive from the weathering of the feldspars (Table 2). SEM analysis and XRD studies of the bulk samples showed that the dominant clay minerals are kaolinite and mixed-layer illite/smectite. Kaolinite exists as pore-filling and grain-coating aggregates (Figures 4e, 4g, 5d, and 5h), postdating the quartz overgrowth phase and predating carbonate cementation (Umar et al., 2011; Zaid, 2012, 2013). The characteristic vermicular texture of kaolinite indicates an origin during early diagenesis (Abouessa and Morad, 2009). SEM analysis indicates that mixed-layer clays (illite/smectite) postdate the quartz cementation (Figures 4f, 5c, 5i, and 5k).

5.5.5. Silica dissolution, carbonate cementation, and grain replacement

The chemistry of the interstitial fluid grows strongly alkaline and unsaturated with silica, and so the major part of the silica overgrowths and, to a lesser extent, parts of the detrital quartz grains were dissolved (QOd) (Figures 4f, 5c, 5j, and 5l).

Carbonate cements, represented by siderite, ankerite, calcite, and dolomite, formed during early diagenesis in the succession. The presence of grain-coating and pore-filling siderite supports this interpretation. The margins of some detrital quartz grains are coated by carbonate cement as seen in thin sections (Figures 4b–4d, 5f, 5g, and 5l). Large pore-spaces that are available for the development of euhedral siderite crystals provide enough evidence for the deposition of siderite during early diagenesis (Lee and Lim, 2008). Minor ferric oxide is formed by oxidation of the siderite (Standard, 1969).

Abouessa and Morad (2009) showed that siderite precipitated at high temperatures with high Fe and low Ca contents. High Fe/Ca (Table 3) also supports the interpretation of the precipitation of siderite cement within the early stage of diagenesis (Lee and Lim, 2008).

The partial development of calcite cement occurs as a mosaic of grains or as superficial pore-filling between grains (Figure 5g). The corroded quartz grains exhibit calcite cement infilling. This evidence suggests the presence of syndepositional calcite cement, which was later replaced by Fe calcite cement during deep burial. The early precipitation of carbonate cement takes place a few centimeters below the sediment–water interface (Bjorlykke, 1983). This type of cementation occurs by exchange of interstitial marine pore water, either by meteoric water or by pore water expelled from the underlying sediments. Recently, tropical shore sediments with intergranular pores have provided favorable space for early carbonate cementation (Bjorlykke, 1983). However,

the thin dark brown mosaic coating of Fe calcite cement on detrital grains may be extrabasinal weathering rinds generated during deep burial (e.g., Walker, 1994).

Some detrital grains and authigenic quartz overgrowths were dissolved and replaced by siderite, ankerite, and/or Fe-calcite cement, and some others were corroded along grain boundaries (Figure 5g).

Generally, the calcareous sandstones do not show any evidence of intergranular pressure solution. Apparently, early carbonate cement may have acted as a buffer between the framework quartz grains and thereby ended grain-to-grain stress. This could be the reason why, even under burial conditions, the intergranular pressure solution effects on detrital grains were not imprinted on these sandstones. Evidence suggests that the replacement of early silica cement by carbonate cements may have resulted in retention of the original intergranular porosity (Figures 4f and 5j).

5.5.6. Illite and chlorite authigenesis

Illite grain-coatings are also characterized as early to mid-authigenic minerals. Illite occurs as fibers, plates, and ribbons overgrowing detrital sheet-like or fibrous illite (Figures 4e, 4g, 5d, 5h, and 5i). Illite coats earlier authigenic kaolinite and silica overgrowths (Figures 4e, 5d, and 5h). High activities of K^+ and H_4SiO_4 support the precipitation of grain-coating illite (Ali and Turner, 1982). Identification of the relative timing of authigenic illite is difficult because the textural relationships between illite and other authigenic minerals were not observed (Sur et al., 2002). The authigenic mineral assemblage and the original sandstone composition indicate the timing of authigenic illite to be during early diagenesis.

Chlorite grain-coatings are also observed to form during early to mid-diagenesis. Kaolinite is coated by chlorite in some samples. This indicates that kaolinite predates chlorite in the Hawkesbury Sandstone. Chlorite and illite formation can be derived from earlier kaolinite (Kim et al., 2007).

5.5.7. Carbonate dissolution and iron oxide cementation

The loss by dissolution of carbonate cement and unstable detrital grains indicates that acid formation water flowed freely through most of the sandstones. Carbonate dissolution is evident in the form of patches of discontinuous carbonate cement and oversized pores (Figure 5g). Meteoric water evidently invaded the sandstones after they had been uplifted and rifted. It is possible that a younger generation of Fe-oxide cements formed at this time at the surface or in the oxidized zone of the water table, which postdated tectonic fractures. The late diagenetic iron oxide (hematite) occurs as pore-filling cement engulfed and stained quartz overgrowth (Figure 5e).

5.6. Paragenesis of the Hawkesbury Sandstone

The inferred paragenetic sequence of the Hawkesbury Sandstone is shown in Figure 15. The sandstones have undergone intense and complex episodes of diagenesis, including early and late diagenesis due to the influence of depositional environment, deep burial, and uplift. The paragenetic sequence is inferred with respect to time by SEM, XRD, and thin-section study.

During early diagenesis, minor amounts of pore-filling and replacement calcite and quartz overgrowths occurred. During burial, mechanical compaction started to reduce pore spaces. Compaction is documented by a tight grain-supported fabric of sandstones. The compaction continued in all sandstones until the precipitation of massive carbonate (especially siderite) in some sandstones ended further compaction and continued up to a late stage in sandstones with little carbonate cement. Mechanical compaction continued from early to late diagenetic stages. Mechanical compaction can be observed by deformation fractures of quartz grains (Figure 4c).

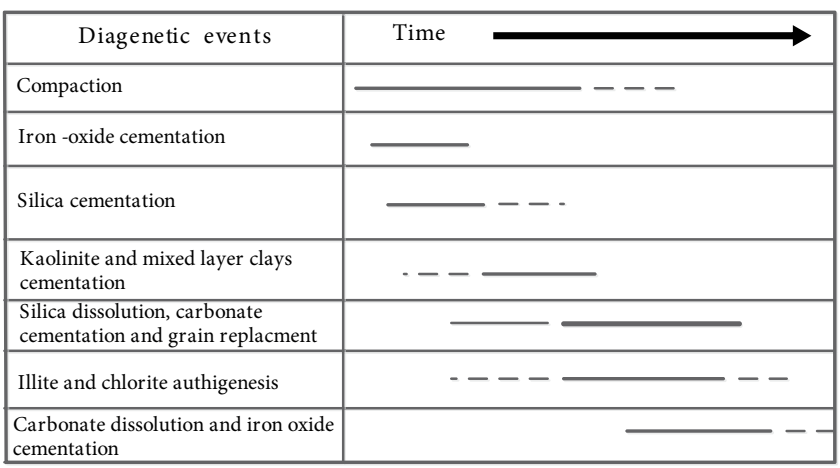

Figure 15. Paragenetic sequence of Hawkesbury Sandstone.

The dissolution and alteration of unstable grains such as feldspar and rock fragments to kaolinite (Figure 5h) was the second important diagenetic event in terms of relative timings. The iron oxides were precipitated at the second diagenetic stage (Figures 4h and 4i). Sources for iron oxide cements might be the liberation of iron by alterations of iron-rich minerals such as hornblende, pyroxene, olivine, magnetite, biotite, and chlorite. Chemical compaction was activated at this stage, allowing pressure solution to provide the silica for quartz cementation. Quartz cement had started to precipitate in open pores before carbonate cementation. This is evidenced by the presence of well-developed quartz overgrowths engulfed and corroded by carbonate (siderite, ankerite, and calcite) cements (Figures 4c, 4h, 5f, 5g, and 5l). Quartz overgrowth is well developed and continued to the late diagenetic stage in samples with little/or rare carbonate cement. The presence and growth of illite and chlorite on kaolinite indicate its later origin than kaolinite (Figures 4e, 4g, 5d, and 5h). The rare mixed-layer clays (illite-smectite) partially embedded and grown on authigenic silica also indicate its later origin than quartz cementation.

The carbonate cementation started slightly later than quartz cementation, as indicated by euhedral quartz overgrowths, which are embedded and partially replaced by siderite, ankerite, and calcite cements (Figures 4f, 5j, and 5l). During the alteration, Mg ions were liberated and reacted to precipitate dolomite overgrowth on calcite cement.

Illite may be formed diagenetically by a number of processes. The most important processes include replacement of feldspar and volcanic fragments, particularly along thin cleavage planes, and illitization of kaolinite (Figures 4e and 4g).

The late diagenetic events were started by the dissolution and replacement of silica by carbonate cements (Figures 4c, 4h, 5g, and 5l). This process typically occurs when the pore waters are undersaturated with respect to carbonate (i.e. the interstitial fluid is strongly alkaline), so the major part of the silica overgrowths and, to a lesser extent, parts of the detrital quartz grains were dissolved.

The late diagenetic events, started by partial leaching of the carbonate cement, occurred when the pore fluids were rendered acidic. During the final stage, a younger generation of Fe-oxide cements (hematite) may have formed following the uplift associated with rifting. The hematite cement may be derived from dissolution or alteration of iron silicates, oxidation of ilmenite and magnetite, and iron released by the replacement of siderite cement (Wolela, 2009). The hematite stains and partially replaces siderite cement, indicating their later origin after siderite cementation (Figure 5e).

5.7. Reservoir control and reservoir quality

The pore type and the main total porosity have been determined from petrographic and SEM studies. Three main pore types have been recognized in the studied samples: 1) primary intergranular macropores, 2) secondary intragranular mesopores, and 3) insignificant intraparticle and intracrystalline micropores. Local occurrences of fractured and vuggy porosity greatly enhance the petrophysical properties of most samples. SEM study shows that the pore interconnection is typically poor to good. Pores generally display irregular pore walls as a result of common dissolution enlargement of pores. Occasional planar pore walls are associated with well-developed quartz overgrowths.

The petrographic analyses reveal a number of controls on porosity development, which include depositional controls (grain size, sorting, roundness, and grain contact) and diagenetic controls (cementation and compaction). The main controls on reservoir quality are carbonate and silica cement and total clay contents (Table 2).

Petrographic examination of grain size, grain sorting, and grain roundness against point-counted porosity shows positive correlations (Tables 1 and 2). However, these positive relations reveal that the overall porosity development is probably controlled by the interplay of cementation and secondary porosity creation. The study reveals that the porosity increases with samples of floating to point contacts and decreases with long, concave–convex, and sutured contacts, as shown in Figures 4a, 4b, and 5c.

The type and nature of cement and pore-occluding cement control porosity development. Modal analysis revealed that point-counted porosity showed positive correlation with authigenic cements (clay, quartz overgrowth, carbonate, and hematite) (Table 2).

Siderite cement has strong control over porosity. Siderite cement, and especially the poikilotopic type, tends to sit in pores, blocking pores throats and thus reducing permeability more than grain-coating cements such as quartz. Samples of less than 20% total carbonate generally have porosities of greater than 12%, while samples possessing greater than 20% total carbonate have less than 10% porosity (Zaid, 2013).

In well logs, helium porosity is present in medium-grained sandstone between 53 and 57.1 m (Well 115), in coarse-grained sandstone between 64 and 67 m (Well 156), and between 227.4 and 239.2 m (Well 42). Rainfall is the main source of groundwater, which is recharged by direct infiltration. The point-counted porosity is high near the surface (i.e. high infiltration rate and good groundwater recharge probability).

The point-counted porosity values range between 0% to 19.3% with an average of 7.78%, while the horizontal permeability values of most samples range between 0.2

md and 22.3 md with average of 7.9 md (i.e. poor to moderate quality). In general, the reservoir quality of the Hawkesbury Sandstone Formation is low-moderate to good and it may contain groundwater, especially near the surface.

The results of this study demonstrate that the cratonic Lachlan Orogen is the main source of the Hawkesbury Sandstone (i.e. sandstones were transported from afar along the rift by the Hawkesbury River). This was indicated by the low percentage of unstable grains such as feldspar and other rock fragments at <8%, the dominance of monocrystalline quartz, and most of the feldspar grains being altered. Siderite cement has strong control over porosity. Samples of less than 20% total carbonate generally have porosities of greater than 12%, while samples possessing greater than 20% total carbonate have less than 10% porosity. Petrophysically, the reservoir quality of the Hawkesbury Sandstone is locally low-moderate to good. The local occurrence of deformation fractures and millimeter-sized vuggy pores following silica and carbonate dissolution greatly enhances the petrophysical properties of many arenites.

Acknowledgments

The authors thank the members of the laboratory of the National Research Center of Egypt for facilitating analytical work for the present research and the journal's reviewers for their very constructive and helpful editorial comments, which helped to improve the manuscript.

References

Aalto KR (1972). Diagenesis of orthoquartzites near Bogota Columbia. J Sediment Petrol 42: 330–340.

Abouessa A, Morad S (2009). An integrated study of diagenesis and depositional facies in tidal sandstones: Hawaz Formation (Middle Ordovician), Murzuq Basin, Libya. J Petrol Geol 32: 39–66.

Abu-Zeid MM, Amer KM, El-Mohammady RA (1989). Petrology, mineralogy and provenance of sandstones of "Nubia" facies in west central Sinai. Earth Science Series 3, Middle East Research Centre, Ain Shams University: 20–34.

Abu-Zeid, MM, Amer KM, Yanni NN, El-Wekeil SS (1991). Petrology, mineralogy and sedimentation of the Paleozoic sequence of Gabal Qattar, Wadi Feiran, Sinai, Egypt. J Geol 34: 145–169.

Agrawal S, Guevara M, Verma SP (2004). Discriminant analysis applied to establish major element field boundaries for tectonic varieties of basic rocks. Int Geol Rev 46: 575–594.

Ahmad I, Chandra R (2013). Geochemistry of loess-paleosol sediments of Kashmir Valley, India: provenance and weathering. J Asian Earth Sci 66: 73–89.

Ahmed AHM, Bhat GM (2006). Petrofacies, provenance and diagenesis of the dhosa sandstone member (Chari Formation) at Ler, Kachchh sub-basin, Western India. J Asian Earth Sci 27: 857–872.

Akarish AIM, El-Gohary AM (2008). Petrography and geochemistry of lower Paleozoic sandstones, East Sinai, Egypt: implications for provenance and tectonic setting. J Afr Earth Sci 52: 43–54.

Al-Habri OA, Khan MM (2008). Provenance, diagenesis, tectonic setting and geochemistry of Tawil sandstone (Lower Devonian in central Saudi Arabia). J Asian Earth Sci 33: 278–287.

Ali AD, Tuner P (1982). Authigenic K-feldspar in the Bromsgrove Sandstone Formation (Triassic) of central England. J Sediment Petrol 52: 187–198.

Amer KM, Abu-Zeid MM, El-Mohammady RA (1989). Particle-size distribution and depositional environment of the sandstones of "Nubia" facies in west central Sinai. Earth Science Series 3, Middle East Research Centre, Ain Shams University: 146–160.

Amireh BS (1991). Mineral composition of the Cambrian-Cretaceous Nubian series of Jordan: provenance, tectonic setting and climatological implication. Sediment Geol 71: 99–119.

Armstrong-Altrin JS, Lee YI, Kasper-Zubillaga, JJ, Carranza-Edwards A, Garcia D, Eby N, Balaram V, Cruz-Ortiz NL (2012). Geochemistry of beach sands along the Western Gulf of Mexico, Mexico: implication for provenance. Chem Erde Geochem 72: 345–362.

Armstrong-Altrin JS, Lee YI, Verma SP, Ramasamy S (2004). Geochemistry of sandstones from the Upper Miocene Kudankulam Formation, southern India: implications for provenance, weathering, and tectonic setting. J Sediment Res 74: 285–297.

Armstrong-Altrin JS, Nagarajan R, Madhavaraju J, Rosalez-Hoz L, Lee YI, Balaram V, Cruz-Martinez A, Avila-Ramirez G (2013). Geochemistry of the Jurassic and upper Cretaceous shales from the Molango Region, Hidalgo, Eastern Mexico: implications of source-area weathering, provenance, and tectonic setting. C R Geosci 345: 185–202.

Armstrong-Altrin JS, Verma SP (2005). Critical evaluation of six tectonic setting discrimination diagrams using geochemical data of Neogene sediments from known tectonic setting. Sediment Geol 177: 115–129.

Ashley GM, Duncan IJ (1977). The Hawkesbury Sandstone: a critical review of proposed environmental models. Journal of the Geological Society of Australia 24: 117–119.

Bakkiaraj R, Nagendra, Nagarajan R, Armstrong-Altrin JS (2010). Geochemistry of sandstones from the Upper Cretaceous Sillakkudi Formation, Cauvery basin, southern India: implication for provenance. J Geol Soc India 76: 453–467.

Bamberry WJ (1992). Stratigraphy and sedimentology of the Late Permian Illawarra Coal Measures, Southern Sydney Basin, New South Wales. PhD, University of Wollongong, Wollongong, Australia.

Basu A (1976). Petrology of Holocene fluvial sand derived from plutonic source rocks: implications to palaeoclimatic interpretation. J Sediment Petrol 46: 694–709.

Basu A, Young S, Suttner LJ, James WC, Mack CH (1975). Re-evaluation of the use of Undulatory extinction and polycrystallinity in detrital quartz for provenance interpretation. J Sediment Petrol 45: 873–882.

Bhatia MR (1983). Plate tectonics and geochemical composition of sandstones. J Geol 91: 611–627.

Bhatia MR, Crook KAW (1986). Trace element characteristics of greywackes and tectonic setting discrimination of sedimentary basins. Contrib Mineral Petr 92: 181–193.

Bjorlykke K (1983). Diagenic reactions in sandstones. In: Parker A, Sellwood BW, editors. Sediment Diagenesis. Dordrecht, the Netherlands: Reidel Publishing, pp. 169–213.

Bjørlykke K, Aagaard P, Dypvik H, Hastings AS, Harper DS (1986). Diagenesis and reservoir properties of Jurassic sandstones from the Haltenbanken area, offshore mid-Norway. In: Spencer AM, Holter E, Cambell CJ, Hanslien PHH, Nysæther E, Ormaasen EG, editors. Habitat of Hydrocarbons of the Norwegian Continental Shelf. London, UK: Graham and Trotman, pp. 275–276.

Bjørlykke K, Egeberg PK (1993). Quartz cementation in sedimentary basins. AAPG Bull 77: 1538–1548.

Blatt H, Middleton G, Murray R (1980). Origin of Sedimentary Rocks. 2nd ed. Englewood Cliffs, NJ, USA: Prentice Hall.

Boles JR, Franks SG (1979). Clay diagenesis in Wilcox sandstones of southwest Texas: implications of smectite diagenesis on sandstone cementation. J Sediment Petrol 49: 55–70.

Burley SD, Kantorowicz JD (1986). Thin section and SEM textural criteria for the recognition of cement-dissolution porosity in sandstones. Sedimentology 33: 587–604.

Chamley H (1990). Clay Sedimentology. Berlin, Germany: Springer-Verlag.

Conaghan PJ (1980). The Hawkesbury Sandstone: gross characteristics and depositional environment. In: Herbert C, Helby R, editors. A Guide to the Sydney Basin. Bulletin No. 26. Maitland, Australia: Geological Survey of New South Wales, pp. 188–253.

Conaghan PJ, Jones JG (1975). The Hawkesbury Sandstone and the Brahmaputra: a depositional model for continental sheet sandstones. Journal of the Geological Society of Australia 22: 275–283.

Conolly JR (1969). Models for Triassic deposition in the Sydney Basin. Special Publication, Journal of the Geological Society of Australia 2: 209–223.

Conolly JR, Ferm JC (1971). Permo-Triassic sedimentation patterns, Sydney Basin, Australia. AAPG Bull 55: 2018–2032.

Cox R, Lowe DR, Cullers RL (1995). The influence of sediment recycling and basement composition on evolution of mudrock chemistry in the southwestern United States. Geochim Cosmochim Ac 59: 2919–2940.

Dapples EC (1979). Diagenesis in sandstones. In: Larsen G, Chinlinger GV, editors. Developments in Sedimentology, Vol. 25, Part A. Amsterdam, the Netherlands: Elsevier, pp. 31–97.

Davis JC (1986). Statistics and Data Analysis in Geology. New York, NY, USA: John Wiley & Sons.

Dehghani MH (1994). Sedimentology, genetic stratigraphy and depositional environment of the Permo-Triassic Succession in the Southern Sydney Basin, Australia. PhD, University of Wollongong, Wollongong, Australia.

Dickinson WR (1970). Interpreting detrital modes of greywacke and arkose. J Sediment Petrol 40: 695–707.

Dickinson WR, Beard LS, Brakenridge GR, Erjavec, JL, Ferguson, RC, Inman KF, Knepp RA, Lindberg FA, Ryberg PT (1983). Provenance of North American Phanerozoic sandstones in relation to tectonic setting. J Geol Soc America 94: 222–235.

Dickinson WR, Suczek CA (1979). Plate tectonics and sandstone compositions. AAPG Bull 63: 2164–2182.

Dott RH (1964). Wackes, greywacke and matrix: what approach to immature sandstone classification. J Sediment Petrol 34: 625–632.

Dutta PK (1987). Origin of rarity of first cycle quartzarenite (abstract). AAPG Bull 71: 551.

Dutton SP (1993). Influence of provenance and burial history on diagenesis of Lower Cretaceous Frontier Formation sandstones, Green River Basin, Wyoming. J Sediment Petrol 63: 665–667.

Dutton SP, Diggs TN (1990). History of quartz cementation in the Lower Cretaceous Travis Peak Formation, East Texas. J Sediment Petrol 60: 191–202.

El-ghali MA, Morad S, Mansburg H, Miguel AC, Sirat M Ogle (2009). Diagenetic alterations to marine transgression and regression in fluvial and shallow marine sandstones of the Triassic Buntsandstein and Keuper sequence, the Paris basin, France. Mar Petrol Geol 26: 289–309.

Fedo CM, Nesbitt HW, Young GM (1995). Unraveling the effects of potassium metasomatism in sedimentary rocks and paleosols with implications for paleoweathering conditions and provenance. J Geol 23: 921–924.

Folk RL (1974). Petrology of Sedimentary Rocks. Austin, TX, USA: Hemphill Publication Co.

Franzinelli E, Potter PE (1983). Petrology, chemistry and texture of modern river sands, Amazon River System. J Geol 91: 23–39.

Gazzi P (1966). Le arenarie del flysch sopracretaceo dell'Appennino modensese: correlazioni con il flysch di Monghidoro. Mineralogica et Petrographica Acta 12: 69–97 (in Italian).

Gentz ML (2006). A pre-mining study of the Hawkesbury Sandstone and aquifer characeristics of potential longwall mining area, Appin area 3. Bachelor of Environmental Science Thesis, University of Wollongong, Wollongong, Australia.

Grevenitz P, Carr P, Hutton A (2003). Origin, alteration and geochemical correlation of Late Permian airfall tuffs in coal measures, Sydney Basin, Australia. Int J Coal Geol 55: 27–46.

Hawkins PJ (1978). Relationship between diagenesis, porosity reduction and oil replacement in Late Carboniferous sandstone reservoirs, Bothamsall oil field, E. Midlands. J Geol Soc London 135: 7–24.

Herbert C (1980). Wianamatta Group and Mittagong Formation. In: Herbert C, Helby R, editors. A Guide to the Sydney Basin. Bulletin No. 26. Maitland, Australia: Geological Survey of New South Wales, pp. 254–272.

Herron MM (1988). Geochemical classification of terrigenous sands and shales from core or log data. J Sediment Petrol 58: 820–829.

Hindrix MS (2000). Evaluation of Mesozoic sandstone composition, southern Junggar, northern Tarim and western Turran basins, northwest China: a detrital record of the ancestral Tian Shan. J Sediment Res 70: 520–532.

Hofer G, Wagreich M, Neuhuber S (2013). Geochemistry of fine-grained sediments of the Upper Cretaceous to Paleogene Gosau Group (Austria, Slovakia): implications for paleoenvironmental and provenance studies. Geosci Front 4: 449–468.

Holail HM, Moghazi AM (1998). Provenance, tectonic setting and geochemistry of greywackes and siltstones of the Late Precambrian Hammamat Group, Egypt. Sediment Geol 116: 227–250.

Houseknecht DW (1988). Intergranular pressure solution in four quartzose sandstones. J Sediment Petrol 58: 228–246.

Hower J, Eslinger EV, Hower ME, Perry EA (1976). Mechanism of burial metamorphism of argillaceous sediments: 1. Mineralogical and chemical evidence. AAPG Bull 87: 725–737.

Ingersoll RV, Bulard TF, Ford RL, Grimn JP, Pickle JP, Sares SW (1984). The effect of grain size on detrital modes: a text of the Gazzi-Dickinson Point Counting method. J Sediment Petrol 54: 103–116.

Ingersoll RV, Suczek CA (1979). Petrology and provenance of Neogene sand from Nicobar and Bengal fans, DSDP sites 211 and 218. J Sediment Petrol 49: 1217–1228.

Jafarzadeh M, Harami RM, Amini A, Mahboubi A, Farzaneh F (2013). Geochemical constraints on the provenance of Oligocene-Miocene siliciclastic deposits (Zivah Formation) of NW Iran: implications for the tectonic evolution of the Caucasus. Arab J Geosci 7: 4245–4263.

Jafarzadeh M, Hosseini-Barzi M (2008). Petrography and geochemistry of Ahwaz Sandstone Member of Asmari Formation, Zagros, Iran: implications on provenance and tectonic setting. Rev Mex de Cien Geol 25: 247–260.

James WC, Mack GH, Suttner LJ (1981). Relative alteration of microcline and sodic plagioclase in semiarid and humid climates. J Sediment Petrol 51: 151–164.

Jin Z, Li F, Cao J, Wang S, Yu J (2006). Geochemistry of Daihai Lake sediments, Inner Mongolia, north China: implications for provenance, sedimentary sorting and catchment weathering. Geomorphology 80: 147–163.

Johnson MD (2006). Solutional weathering of the Hawkesbury Sandstone and cliff instability. Bachelor of Environmental Science Thesis, University of Wollongong, Wollongong, Australia.

Keller WD (1956). Clay minerals as influenced by environments of their formation. AAPG Bull 40: 2689–2710.

Khanchuk AI, Nevstruev VG, Berdnikov NV, Nechaev VP (2013). Petrochemical characteristics of carbonaceous shales in the eastern Bureya massif and their precious-metal mineralization. Russ Geol Geophys 54: 627–636.

Kim JC, Lee YI, Hisada KI (2007). Depositional and compositional controls on sandstone diagenesis, the Tetori Group (Middle Jurassic-Early Cretaceous), central Japan. Sediment Geol 195: 183–202.

Kroonenberg SB (1994). Effects of provenance, sorting and weathering on the geochemistry of fluvial sands from different tectonic and climatic environments. In: Proceedings of the 29th International Geological Congress, Part A, Kyoto, Japan, 1992. Utrecht, the Netherlands: VSP Publishing, pp. 69–81.

Laird MG (1972). Sedimentology of Greenland Group in the Paparoa Range, West Coast, South Island, New Zealand. J Geol Geophys 15: 372–393.

Le Bas MJ, Le Maitre RW, Streckeisen A, Zanettin B (1986). A chemical classification of volcanic rocks based on the total alkali-silica diagram. J Petrol 27: 745–750.

Lee YI, Lim DH (2008). Sandstone diagenesis of the Lower Cretaceous Sindong Group, Gyeongsang Basin, southeastern Korea: implications for compositional and paleoenvironmental controls. Island Arc 17: 152–171.

Lonnie TP (1982). Mineralogic and chemical composition of marine and nonmarine transitional clay beds on south shore of Long Island, New York. J Sediment Petrol 52: 529–536.

McBride EF (1963). A classification of common sandstones. J Sediment Petrol 33: 664–669.

McLennan SM, Hemming S, McDaniel DK, Hanson GN (1993). Geochemical approaches to sedimentation, provenance, and tectonics. GSA Special Papers 284: 21–40.

McLennan SM, Taylor SR, McCulloch MT, Maynard JB (1990). Geochemical and Nd-Sr isotopic composition of deep-sea turbidites: crustal evolution and plate tectonic associations. Geochim Cosmochim Ac 54: 2015–2050.

Miall AD, Jones BG (2003). Fluvial architecture of the Hawkesbury Sandstone (Triassic), near Sydney, Australia. J Sediment Res 73: 531–545.

Morad S (1998). Carbonate cementation in sandstones: distribution patterns and geochemical evolution. In: Morad S, editor. Carbonate Cementation in Sandstones. Gent, Belgium: International Association of Sedimentologists Special Publication, pp. 1–26.

Morad S, Ketzer JM, De Ros F (2000). Spatial and temporal distribution of diagenetic alterations in siliciclastic rocks: implications for mass transfer in sedimentary basins. Sedimentology 47: 95–120.

Nath BN, Kunzendorf H, Pluger WL (2000). Influence of provenance, weathering and sedimentary processes on the elemental ratio of the fine-grained fraction of the bed load sediments from the Vembanad Lake and the adjoining continental shelf, southwest Coast of India. J Sediment Res 70: 1081–1094.

Naughton JJ, Terada K (1954). Effect of eruption of Hawaiian volcanoes on the composition and carbon isotopic composition of associated volcanic and fumarolic gases. Science 120: 580–581.

Nesbitt HW, Fedo CM, Young GM (1997). Quartz and feldspar stability, steady and non-steady-state weathering, and petrogenesis of siliciclastic sands and muds. J Geol 105: 173–192.

Nesbitt HW, Young GM (1982). Early Proterozoic climates and plate motions inferred from major element chemistry of lutites. Nature 299: 715–717.

Nesbitt HW, Young GM (1984). Prediction of some weathering trends of plutonic and volcanic rocks based on thermodynamic and kinetic considerations. Geochim Cosmochim Ac 48: 1523–1534.

Nowrouzi Z, Moussavi-Harami R, Mahboubi A, Gharaie MHM, Ghaemi F (2013). Petrography and geochemistry of Silurian Niur sandstones, Derenjal Mountains, East Central Iran: implications for tectonic setting, provenance and weathering. Arab J Geosci 7: 2793–2813.

Osae S, Asiedu DK, Banoeng-Yakubo B, Koeberl C, Dampare SB (2006). Provenance and tectonic setting of Late Proterozoic Buem sandstones of southeastern Ghana: Evidence from geochemistry and detrital modes. J Asian Earth Sci 44: 85–96.

Pettijohn FJ (1963). Chemical Composition of Sandstones-Excluding Carbonate and Volcanic Sands. Reston, VA, USA: USGS Professional Paper.

Pettijohn FJ (1975). Sedimentary Rocks. 2nd ed. New York, NY, USA: Harper and Row.

Pettijohn FJ (1984). Sedimentary Rocks. 3rd ed. New Delhi, India: CBS Publishers & Distributors.

Pettijohn FJ, Potter PE, Siever R (1972). Sand and Sandstones. 1st ed. New York, NY, USA: Springer-Verlag.

Pettijohn FJ, Potter PE, Siever R (1987). Sand and Sandstones. 2nd ed. New York, NY, USA: Springer-Verlag.

Potter PE (1978). Petrology and chemistry of modern Big River sands. J Geol 86: 423–449.

Retallack GJ (1999). Postapocalyptic greenhouse paleoclimate revealed by earliest Triassic paleosols in the Sydney Basin, Australia. Geol Soc Am Bull 111: 52–70.

Rodrigo DL, Luiz FDR (2002). The role of depositional setting and diagenesis on the reservoir quality of Devonian sandstones from the Solimones Basin, Brazilian Amazonia. Mar Petrol Geol 19: 1047–1071.

Rollinson HR (1993). Using Geochemical Data: Evaluation, Presentation, Interpretation. London, UK: Longman.

Roser BP, Cooper RA, Nathan S, Tulloch AJ (1996). Reconnaissance sandstone geochemistry, provenance, and tectonic setting of the lower Paleozoic terranes of the West Coast and Nelson, New Zealand. New Zealand J Geol Geophys 39: 1–16.

Roser BP, Korsch RJ (1986). Determination of tectonic setting of sandstone-mudstone suites using SiO_2 content and K_2O/Na_2O ratio. J Geol 94: 635–650.

Roser BP, Korsch RJ (1988). Provenance signatures of sandstone-mudstone suites determined using discrimination function analysis of major element data. Chem Geol 67: 119–139.

Rust BR, Jones BG (1987). The Hawkesbury Sandstone south of Sydney, Australia: Triassic analogue for the deposit of a large braided river. J Sediment Petrol 57: 222–233.

Saunders AD, England RW, Reichow MK, White RV (2005). A mantle plume origin for the Siberian traps: uplift and extension in the West Siberian Basin, Russia. Lithos 79: 407–424.

Schwab FL (1975). Framework mineralogy and chemical composition of continental margin type sandstone. Geology 3: 487–490.

Selvaraj K, Chen CTA (2006). Moderate chemical weathering of subtropical Taiwan: constraints from solid-phase geochemistry of sediments and sedimentary rocks. J Geol 14: 101–116.

Shadan M, Hosseini-Barzi M (2013). Petrography and geochemistry of the Ab-e-Haji Formation in central Iran: implications for provenance and tectonic setting in the southern part of the Tabas block. Rev Mex Cien Geol 30: 80–95.

Spry AH (2000). The Hawkesbury Sandstone: its origins and later life. In: McNally GH, Franklin BJ, editors. Sandstone City: Sydney's Dimension Stone and other Sandstone Geomaterials: Proceedings of a Symposium, University of Technology, Sydney, Australia.

Standard JC (1969). Hawkesbury Sandstone. Journal of the Geological Society of Australia 16: 407–417.

Sur KH, Lee YI, Hisada KI (2002). Diagenesis of the Lower Cretaceous Kanmon Group sandstones, SW Japan. J Asian Earth Sci 20: 921–935.

Suttner LJ, Basu A, Mack GH (1981). Climate and the origin of quartz arenites. J Sediment Petrol 51: 235–246.

Suttner LJ, Dutta PK (1986). Alluvial sandstone composition and paleoclimate, I. Framework mineralogy. J Sediment Petrol 56: 329–345.

Taylor JM (1950). Pore-space reduction in sandstones. AAPG Bull 34: 701–716.

Taylor SR, McLennan SM (1985). The Continental Crust: Its Composition and Evolution. Oxford, UK: Blackwell.

Trevena AS, Nash WP (1981). An electron microprobe study of detrital feldspar. J Sediment Petrol 51: 137–150.

Tsuzuki Y, Kawabe I (1983). Polymorphic transformations of kaolin minerals in aqueous solutions. Geochim Cosmochim Ac 47: 59–66.

Umar M, Friis H, Khan A, Kassi, AM, Kasi AK (2011). The effects of diagenesis on the reservoir characters in sandstones of the Late Cretaceous Pab Formation, Kirthar Fold Belt, southern Pakistan. J Asian Earth Sci 40: 622–635.

Vdačný M, Vozárová A, Vozár J (2013). Geochemistry of the Permian sandstones from the Malužiná Formation in the Malé Karpaty Mts (Hronic Unit, Western Carpathians, Slovakia): implications for source-area weathering, provenance and tectonic setting. Geol Carpath 64: 23–38.

Veevers JJ (1984). Phanerozoic Earth History of Australia. Oxford, UK: Clarendon Press.

Veevers JJ (2006). Updated Gondwana (Permian–Cretaceous) earth history of Australia. Gondwana Res 9: 231–260.

Veevers JJ, Conaghan PJ, Powell CM (1994). Eastern Australia, Permian–Triassic Pangean Basins and Foldbelts along the Panthalassan Margin of Gondwanaland. Boulder, CO, USA: Geological Society of America.

Verma SP, Armstrong-Altrin JS (2013). New multi-dimensional diagrams for tectonic discrimination of siliciclastic sediments and their application to Precambrian basins. Chem Geol 355: 117–180.

Verma SP, Guevara M, Agrawal S (2006). Discriminating four tectonic settings: five new geochemical diagrams for basic and ultrabasic volcanic rocks based on log-ratio transformation of major-element data. J Earth System Sci 115: 485–528.

Walderhaug O (1994). Temperatures of quartz cementation in Jurassic sandstones from Norwegian continental shelf-evidence from fluid inclusion. J Sediment Res 64: 311–324.

Walker TR (1994). Formation of red beds in moist tropical climate. A hypothesis. AAPG Bull 84: 633–638.

Weltje GJ, Meijer XD, De Boer PL (1998). Stratigraphic inversion of siliciclastic basin fills: a note on the distinction between supply signals resulting from tectonic and climatic forcing. Basin Res 10: 129–153.

White RV, Saunders AD (2005). Volcanism, impact and mass extinctions: incredible or credible coincidences? Lithos 79: 299–316.

Wolela A (2009). Diagenetic evolution of the Ansian-Pliensbachian Adigrat Sandstone, Blue Nile Basin, Ethiopia. J Afr Earth Sci 56: 29–42.

Zaid SM (2012). Provenance, diagenesis, tectonic setting and geochemistry of Rudies sandstone (Lower Miocene), Warda Field, Gulf of Suez, Egypt. J Afr Earth Sci 66–67: 56–71.

Zaid SM (2013). Provenance, diagenesis, tectonic setting and reservoir quality of the sandstones of the Kareem Formation, Gulf of Suez, Egypt. J Afr Earth Sci 85: 31–52.

Zhang J, Qin L, Zhongjie Z (2008). Depositional facies, diagenesis and their impact on the reservoir quality of Silurian sandstones from Tazhong area in central Tarim basin, western China. J Asian Earth Sci 33: 42–60.

Zhang KL (2004). Secular geochemical variations of the Lower Cretaceous siliciclastic from central Tibet (China) indicate a tectonic transition from continental collision to back-arc rifting. Earth Plan Sci Lett 229: 73–89.